UNIVERSITY OF CALIFORNIA
RIVERSIDE

Investigating Mechanisms of Oriented Cell Divisions in the Root Ground Tissue of *Arabidopsis thaliana*

A Dissertation submitted in partial satisfaction
of the requirements for the degree of

Doctor of Philosophy

in

Cell, Molecular, and Developmental Biology

by

Jason B. Goff

September 2021

Dissertation Committee:

Dr. Jaimie M. Van Norman, Chairperson
Dr. Dawn Nagel
Dr. Patricia Springer

The Dissertation of Jason B. Goff is approved by:

_____

_____

_____

Committee Chairperson

University of California, Riverside

ACKNOWLEDGEMENTS

Initial Research Evaluation Committee:

Jaimie M. Van Norman

Jeffery Bachant

Carolyn Rasmussen

Anandasankar Ray

Qualifying Exam Committee:

Dawn Nagel

Ted Karginov

Carolyn Rasmussen

Patricia Springer

Jason Stajich

Dissertation Committee:

Jaimie M. Van Norman

Dawn Nagel

Patricia Springer

The text of this dissertation, in part, is a reprint of the material as it appears in bioRxiv, 2021. The coauthor Jaimie M. Van Norman listed in that publication directed and supervised the research which forms the basis for this dissertation.

Funding:

UC, Riverside (J.M.V.N) Initial complement funds

NSF CAREER (J.M.V.N.) #1751385

USDA-NIFA-CA-R-BPS-5156-H (J.M.V.N.)

Note from Author:

Many thanks to my family, friends, and colleagues who offered their support and encouragement throughout the years. This dissertation is dedicated to my father Larry Goff who passed away a few months prior to starting at UCR.

ABSTRACT OF THE DISSERTATION

Investigating Mechanisms of Oriented Cell Divisions in the
Root Ground Tissue of *Arabidopsis thaliana*

by

Jason B. Goff

Doctor of Philosophy, Graduate Program in Cell, Molecular, and Developmental Biology
University of California, Riverside, September 2021
Dr. Jaimie M. Van Norman, Chairperson

In multicellular eukaryotes, coordination of cell division and differentiation is critical for tissue patterning and organ development. In plants, oriented cell division, directional cell signaling, and cell polarity have been proposed to coordinate these developmental processes. The Arabidopsis root provides an excellent model for study of oriented cell divisions, as the nearly invariant organization of the root allows for visualization of defects in cell divisions when examining gene function through a reverse genetics approach. Cell-cell communication has been implicated in root oriented cell divisions, for instance, a transmembrane receptor kinase named INFLORESCENCE AND ROOT APICES RECEPTOR KINASE (IRK) is polarly localized and functions to restrict root width and inhibit specific cell divisions in the endodermis. Here, we further investigate IRK function by exploring whether cell identity is sufficient for IRK polar localization, misregulation of cell cycle components in *irk*, and transcriptional regulation of *IRK* during endodermal development. Additionally, we examined the function of the receptor most closely related to IRK, PXY/TDR CORRELATED 2 (PXC2) to understand how these proteins operate in directional cell-cell signaling and root development. *pxc2*

roots have increased root width, indicating that PXC2 and IRK function in this process. Compared to either single mutant, *irk pxc2* roots have an enhanced phenotype with further increases in root width and endodermal cell divisions indicating redundant activities of these receptors. The double mutant also exhibits abnormal root growth, suggesting broader functions of PXC2 and IRK in the root. Finally, we begin to characterize a dominant mutant phenotype called *crazy cortex* (*crz*), which exhibits periclinal divisions in the presumptive cortex cell layer, which does not normally divide periclinally in the root. Together, these studies seek to understand how oriented divisions are restricted to ensure stereotypical root tissue and organ development.

TABLE OF CONTENTS

CHAPTER I: Control of oriented and formative cell divisions are required for maintenance of tissue and organ patterning 1

References 11

CHAPTER II: Exploring the relationship between IRK and endodermal cell division and IRK protein accumulation in ground tissue mutants 15

Introduction 15

Results 18

Examining transcriptional regulation of *IRK* during MC development 18

IRK localization is informed by positional cues not cell identity 20

pCYCD6;1 is misexpressed in *irk* mutants 23

Discussion 25

Experimental Procedures 27

References 30

CHAPTER III: Polarly localized receptor-like kinases PXC2 and IRK act redundantly during Arabidopsis root development in the radial axis 32

Introduction 32

Results 37

PXC2-GFP is polarly localized root tissues 37

Mutant alleles of *PXC2* have an enlarged stele area 40

PXC2 and IRK have redundant functions in restricting stele area and repressing endodermal longitudinal anticlinal cell divisions 44

irk pxc2 double mutants exhibit a root growth defect 46

PXC2 is not functionally equivalent to IRK 48

Discussion 50

Experimental Procedures 56

Acknowledgements 63

References 65

CHAPTER IV: Characterizing *crazy cortex*, a phenotype in *Arabidopsis* with defects in root ground tissue patterning 69

Introduction 69

Results 71

crazy cortex roots have defects in ground tissue periclinal divisions 71

CYCD6;1 is expressed during the periclinal divisions in *crz* ground tissue 75

crz can serve as a model to further understand IRK polarity requirements 77

Discussion 80

Experimental Procedures 82

References 85

CHAPTER V: Discussion and future directions 87

Identifying the causative gene(s) for the abnormal *crz* phenotype 87

Polar localization of IRK and PXC2 to specific PM domains 88

Expression of *IRK* during MC development 90

Probing function of IRK, PXC2 and other closely related LRR-RLKs 91

References 93

LIST OF FIGURES

Figure 1.1: Root cellular organization, ground tissue development, cell division planes, and plasma membrane polar domains in root cells 2

Figure 1.2: IRK-GFP accumulation shows polar localization to distinct plasma membrane domains 7

Figure 1.3: *irk* roots have increased stele area, and additional periclinal and longitudinal anticlinal divisions in the endodermis 9

Figure 2.1: Expression of *pIRK*:*erGFP* is unchanged in the endodermis prior dividing periclinally to generate MC 19

Figure 2.2: IRK localization is not dependent on cell identity 22

Figure 2.3: Misexpression of *pCYCD6;1* in *irk* mutants 24

Figure 3.1: PXC2 is polarly localized in root cell types 34

Figure 3.2: *PXC2* promoter activity and PXC2-GFP accumulation across the root developmental zones 39

Figure 3.3: *PXC2* gene structure and expression analyses 41

Figure 3.4: *pxc2-3* and *pxc2-1*/*canar-1* roots have similar abnormal root phenotypes 43

Figure 3.5: Abnormal pxc2 phenotype and enhanced phenotype of irk pxc2 double mutant 45

Figure 3.6: Disorganization of *irk-4 pxc2-3* roots is rescued back to *irk-4* by expression of *pPXC2:PXC2:GFP* and *pxc2-3* and *irk-4* single mutant root growth phenotypes 47

Figure 3.7: *irk pxc2* roots exhibit abnormal root growth phenotypes 49

Figure 3.8: PXC2 partially rescues abnormal root phenotypes in *irk* 51

Figure 3.9: Summary of IRK and PXC2 function to restrict stele area and endodermal LADs and phenotypic outcomes 53

Figure 4.1: *crz* roots have defects in number of ground tissue cell layers 73

Figure 4.2: *pCYCD6;1* is expressed in the cortex during periclinal divisions in *crz* 76

Figure 4.3: IRK-GFP polar localization in *crz* demonstrates how positional information determines IRK polarity 78

CHAPTER I: Control of oriented and formative cell divisions are required for maintenance of tissue and organ patterning

In multicellular organisms, coordination of cell division and differentiation is essential for cellular, tissue and organ function (Alim et al., 2012). In plants, asymmetric cell divisions, division plane orientation, and cell polarity are especially important due to cells being fixed in place by a rigid cell wall (Rasmussen and Bellinger., 2018). The Arabidopsis root consists of layers of tissues that surround the central stele, which includes the pericycle and the interior vasculature (Figure 1.1A) (Dolan et al., 1993). Peripheral to the stele in the radial axis, is the ground tissue (GT), which consists of the endodermis and cortex, then the epidermis and lateral root cap (Figure 1.1A, B). Root cell types are continuously formed through a series of asymmetric, formative cell divisions within the stem cell niche. These divisions are controlled by a central organizing center, called the quiescent center (QC), which contains cells that infrequently divide (Doerner., 1998). The QC is surrounded by initial cells, which asymmetrically divide to generate each of the various root cell types (Dolan et al., 1993; Benfey and Scheres, 2000).

The formative divisions of initial cells occur at specific orientations, as placement of the division plane determines the fate of the resulting daughter cell (Rasmussen and Bellinger, 2018; Facette et al., 2019). In the root, cell division planes can be categorized into three distinct types. First, periclinal divisions occur parallel to the root's surface and generate an additional cell layer in the radial axis and longitudinal axis. Then there are two types of anticlinal cell divisions: transverse anticlinal divisions, which occur

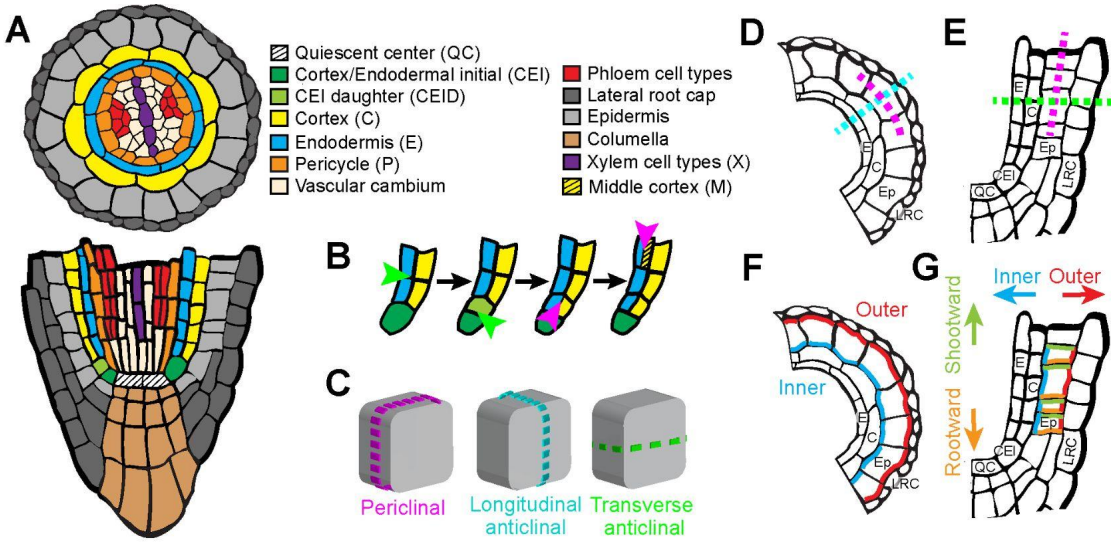

Figure 1.1 Root cellular organization, ground tissue development, cell division planes, and plasma membrane polar domains in root cells. (A) Schematic of the Arabidopsis thaliana root tip (top) transverse and (bottom) median longitudinal sections, with cell types listed (right). (B) Ground tissue development with green arrows indicating transverse anticlinal divisions and magenta arrows indicating periclinal divisions. (C) Division planes of an individual cell (grey box) with division site indicated by colored dashed line. Schematic sections of Arabidopsis root tip illustrating the three division planes in the root tip in the (D) transverse and (E) median longitudinal plane. Schematic sections of the Arabidopsis root tip showing plasma membrane domains in the (F) transverse and (G) median longitudinal plane. (Figure uses images found in Campos et al., 2020).

perpendicular to the root's surface and increase cell number only in the longitudinal axis, and longitudinal anticlinal divisions (LADs), which also occur perpendicular to the root's surface, but are only observed in the transverse axis of the root and result in additional cells in a radial ring of cells (Figure 1.1C, D) (Van Norman., 2016) . The orientation of root cell divisions appear tightly controlled during root development, for example, the root ground tissue develops through a series of formative cell divisions that occur in a precise order and orientation (Dolan et al. 1993). After seed germination, perpetuation of the two ground tissue cell types is maintained by formative cell division of the cortex/endodermal initial cell (CEI), which is immediately adjacent to the QC. The CEI first undergoes an anticlinal, formative division to generate the cortex/endodermal initial daughter (CEID) cell (Dolan et al., 1993). The CEID will later divide periclinally to generate the two cell layers of the ground tissue, the endodermis adjacent to the stele and the cortex next to the epidermis (Figure 1.1A ,B). Later in development, the endodermis can divide periclinally to generate an additional ground tissue layer called middle cortex (Baum et al., 2002; Cui and Benfey, 2009; Cui, 2016). However, cortex cells do not undergo periclinal divisions to form additional ground tissue cell layers, which suggests strict inhibition of periclinal cell divisions in the cortex. Cell types throughout the root's meristematic zone proliferate in longitudinal files through transverse anticlinal divisions. However, longitudinal anticlinal divisions rarely occur with these divisions generating additional cells of the same type in the radial axis (surrounding the stele). Following proliferation, cells shootward of the meristematic zone will rapidly elongate, a process which constitutes the majority of root lengthening (Hodge et al., 2009). Differential cell elongation across the root is responsible for directional growth through tropic responses to the root's environment. In order to coordinate cell division and elongation with

environmental cues and during normal root growth, cell-cell communication must occur to ensure coordinated growth and development, and ultimately normal root formation and function (van den Berg et al., 1995, 1997; Nakajima and Benfey, 2002; Van Norman et al., 2011). The signaling pathways by which cells communicate with each other to coordinate these processes is an important topic in developmental biology. Understanding how cells relay and perceive this information may lead to a greater understanding of how precise control of cell division orientation is maintained during development.

In plant development, positional information is critical to the identity or specification of a cell. This means the orientation of formative cell divisions and specification of daughter cell fate are closely linked and there is evidence that extrinsic factors are important for these processes. For example, SHORT ROOT (SHR), a key transcriptional regulator of ground tissue formative divisions and endodermal cell identity, is expressed in the stele and moves outward to regulate GT development (Helariutta et al., 2000; Nakajima et al., 2001; Gallagher et al., 2004; Koizumi et al., 2012). Additionally, cell ablation studies have shown that root stem cell maintenance and daughter cell differentiation relies upon extrinsic cues from neighboring cells (van den Berg et al., 1995, 1997; Kidner et al., 2000; Marhava et al., 2019). Perception of these extrinsic cues is implied in this hypothesis, and may be predicted to occur at the plasma membrane (PM). Examples of membrane associated signaling proteins that relay extrinsic cues necessary for development include BREAKING OF ASYMMETRY IN THE STOMATAL LINEAGE (BASL) (Dong et al., 2009), POLAR (Pillitteri et al., 2011), and BREVIS RADIX-LIKE 2 (BRXL2) (Rowe et al., 2019), these proteins are required to

direct cell division plane orientation during stomatal development. In maize, two transmembrane receptors, PANGLOSS1 (PAN1) and PAN2 are polarly localized and required for the formative cell division during stomatal development (Cartwright et al., 2009; Zhang et al., 2012; Facette et al., 2015). PAN1 and PAN2 are part of a large family of transmembrane receptors in plants, called leucine-rich repeat receptor-like kinases (LRR-RLKs) (Shiu and Bleecker, 2001, 2003; Lehti-Shiu and Shiu, 2012), which are proposed to perceive extracellular signals and activate downstream signaling pathways, and may play critical roles in cell-cell signaling during development, yet many of these proteins lack functional characterization *in planta*.

A recent example of an LRR-RLK that limits the occurrence of formative cell divisions in the Arabidopsis root is INFLORESCENCE AND ROOT APICES RECEPTOR KINASE (IRK) (Campos et al., 2020). IRK was identified as a candidate protein involved in ground tissue formative cell divisions based on its expression in the endodermis upon SHR induction (Sozzani et al., 2010). Examination of a transcriptional reporter indicated that *IRK* promoter activity (*pIRK:erGFP*) was predominantly found in the CEI, CEID, endodermis, and pericycle. To determine IRK protein localization, a translational reporter was constructed (*pIRK:IRK:GFP*) and expressed in WT plants. Upon examination, IRK-GFP was predominantly detected in the CEI, CEID, endodermis, and pericycle (Figure 1.2 A, B). IRK-GFP was also weakly detected in the cortex and epidermis, though *pIRK:erGFP* expression was not observed in these cell types (Campos et al., 2020). Close examination of its accumulation indicated that IRK-GFP was not uniformly distributed in the PM of these cell types, and instead showed lateral localization towards the cortex in the endodermis, however IRK-GFP appeared polarized to the at the top

and bottom of the CEI/CEID, and appeared non-polar in middle cortex cells (Figure 1.2 A, B). As IRK-GFP is localized to distinct plasma membrane domains in cells with different identities, it suggests that cell identity influences IRK localization.

Cell polarity can be defined as an asymmetry in partitioning of cellular components and/or cell morphology. In the Arabidopsis root, cell polarity can be conceptualized by partitioning localization to distinct "sides" of the cell (Van Norman., 2016). As the root is composed of cells that are primarily cuboidal in shape, proteins with apical/basal localization are at the shootward/rootward side of the cell with the shootward side being towards the shoot and rootward being towards the root tip (Figure 1.1 G). Additionally, lateral polarity occurs if the protein is localized towards the stele (inner polarity) or towards the surface or environment (outer polarity) (Figure 1.1F, G). Therefore, when describing IRK-GFP localization in the CEI/CEID, we would refer to this as rootward and/or shootward localization and IRK-GFP localization in the endodermis would be described as outer polar localization. Lateral polarity can also be observed if protein accumulates towards cells adjacent to each other within a ring of cells, with observation of protein accumulation visible when viewing the root as a transverse section.

To determine IRK-GFP localization in individual root cell types, cell type-specific promoters were used to drive its expression. This helped to eliminate overlapping fluorescent signals from adjacent cell types. When IRK was expressed in WT roots from the *SCARECROW* transcriptional reporter (*pSCR*), which is specifically active in the endodermis, CEI/CEID, and QC, IRK-GFP accumulated to the outer polar domain of

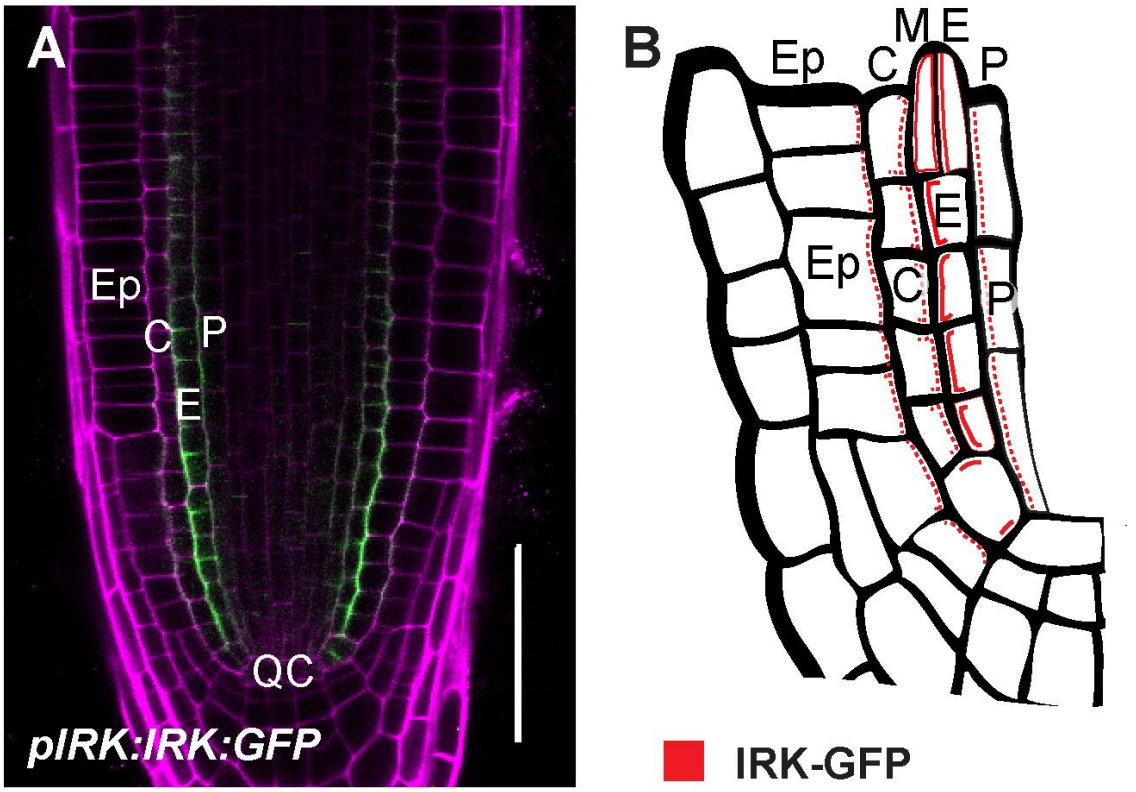

Figure 1.2 IRK-GFP accumulation shows polar localization to distinct plasma membrane domains. (A) Confocal micrograph showing a root (5 dps) showing localization of IRK-GFP driven by *pIRK*, with green fluorescent protein (GFP) and stained with propidium iodide (PI) to show cell outlines. (B) Schematics summarizing IRK-GFP localization when driven by *pIRK*, dotted lines represent weaker signal. Abbreviations: Ep - Epidermis, C - Cortex, E - Endodermis, P - Pericycle, QC - quiescent center, M - Middle Cortex. Scale bar: 50μm.

endodermal cells, with rootward/shootward localization in the CEI and CEID cells (Campos et al., 2020). This is similar to our observations of IRK-GFP localization with the endogenous reporter *pIRK:IRK:GFP* (Figure 1.2A, B). We also observed IRK-GFP localization in the cortex and epidermis using the *CORTEX2* (*pCO2*) and *WEREWOLF* (*pWER*) promoters respectively (Lee and Schiefelbein, 1999; Heidstra et al., 2004; Paquette and Benfey, 2005), and found that IRK-GFP was polarly localized to the inner polar domain when misexpressed in these cell types (Campos et al., 2020). Furthermore, as *pCO2* is also expressed in middle cortex cells, we observed non-polar IRK-GFP localization in the roots expressing *pCO2:IRK:GFP*, which indicates that non-polar accumulation is independent of its expression in the endodermal mother cell (Campos et al., 2020). These results suggest that IRK-GFP polar localization is informed by cell identity and not through global cues (Yoshida et al., 2019), however further investigation was performed to determine if cell identity alone was sufficient to inform IRK localization (see Chapter III).

Given expression and polar localization of IRK in the root GT and the differences in polar localization of IRK when expressed in different root cell types, we predicted that IRK functions in GT development. Upon examination, we found that *irk-1* (Salk_038787 (Alonso et al., 2003)) had abnormal divisions in the GT lineage. However, as the penetrance of the *irk-1* allele was low, we generated a putative null allele via CRISPR-Cas9 mutagenesis that was named *irk-4*. Similar to *irk-1,* endodermal cells of *irk-4* divide early compared to WT to generate middle cortex (MC). In addition, *irk-4* CEI cells terminally divide prematurely, which results in the loss of a persistent CEI. Through examination of serial optical transverse sections of *irk-4* roots, we observed that *irk-4*

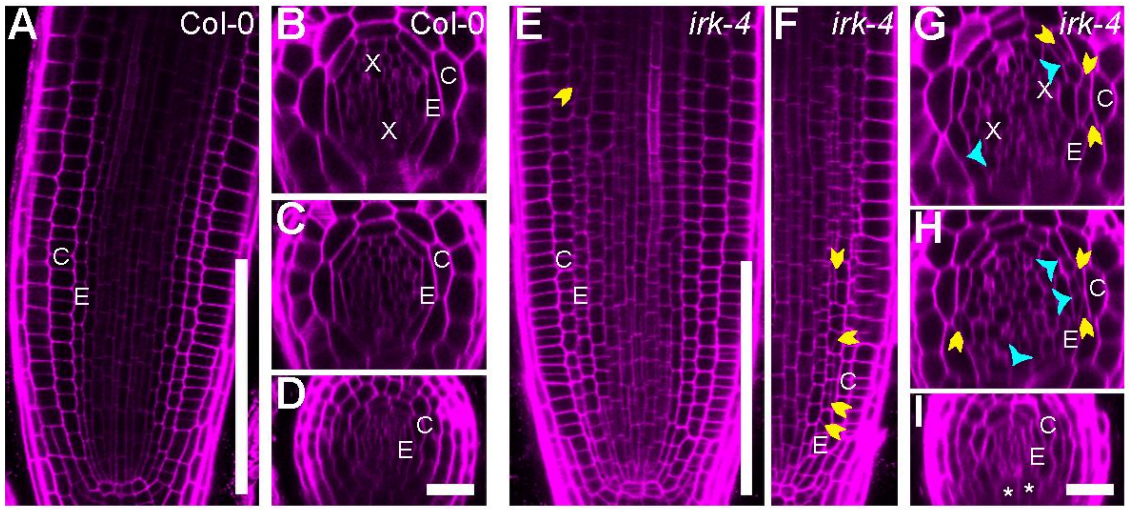

Figure 1.3 *irk* roots have increased stele area, and additional periclinal and longitudinal anticlinal divisions in the endodermis. (A–H) Confocal micrographs of roots at 6 dps stained with PI (magenta). (A and E) Longitudinal root sections, note abnormal timing and orientation of periclinal endodermal cell divisions (yellow arrowheads) in *irk-4*. (B–D and F–H) Transverse sections of roots at (B) and (F) 120 µm, (C) and (G) 60 µm, and (D) and (H) 10 µm above the QC. Note endodermal LADs (cyan arrowheads), endodermal cells, and all daughter cells traced and highlighted to increase visibility. Scale bars: 50 µm in (A), and (E), and 20 µm in (B)–(D), and (G)–(H). Abbreviations: (E) - endodermis, (C) - cortex, (X) xylem. Figure adapted from (Campos et al., 2020).

had between 9 and 14 endodermal cells in transverse sections of the meristematic zone, as compared to WT with only 8 to 11 endodermal cells per transverse section (Figure 1.3). These additional cells in *irk-4* are the result of endodermal LADs, which occur more frequently in endodermal cells aligned with the xylem poles (Campos et al., 2020). Furthermore, when comparing *irk-4* to WT, we also observed an increased stele area at 4 days post stratification (dps) at multiple distances shootward from the QC. These data indicate that IRK functions to inhibit specific divisions in the GT and restrict stele area.

In this work, we aim to determine if polar localization of IRK is informed primarily by the identity of the cell in which it is expressed. Additionally, we examine expression of *IRK* prior to initiation of MC development and investigate the expression of a known, GT specific cell cycle regulator in *irk* mutants. We also report on the most closely related gene to *IRK*, *PXY-TDR CORRELATED 2* (*PXC2*), and our findings that these two gene products are functionally redundant in restriction of endodermal LADs and stele area. Finally, we discuss a novel mutant phenotype named *crazy cortex* (*crz*) in which a dominant genomic lesion unexpectedly results in periclinal divisions in the cortex. Together, this work demonstrates links between laterally polarized receptor proteins and oriented cell divisions in the root and indicates periclinal divisions in the cortex are genetically controlled and actively prevented. Through work detailed in this dissertation, we can begin to further understand the requirements for restricting formative and oriented cell divisions, which is essential for precise patterning of organs and tissues.

REFERENCES

Alim, K., Hamant, O., and Boudaoud, A. (2012). Regulatory role of cell division rules on tissue growth heterogeneity. Front. Plant Sci. **3**: 174.

Alonso, J.M. et al. (2003). Genome-wide insertional mutagenesis of Arabidopsis thaliana. Science **301**: 653–657.

Baum, S.F., Dubrovsky, J.G., and Rost, T.L. (2002). Apical organization and maturation of the cortex and vascular cylinder in Arabidopsis thaliana (Brassicaceae) roots. Am. J. Bot. **89**: 908–920.

Benfey, P.N. and Scheres, B. (2000). Root development. Curr. Biol. **10**: R813–5.

van den Berg, C., Weisbeek, P., and Scheres, B. (1998). Cell fate and cell differentiation status in the Arabidopsis root. Planta **205**: 483–491.

van den Berg, C., Willemsen, V., Hage, W., Weisbeek, P., and Scheres, B. (1995). Cell fate in the Arabidopsis root meristem determined by directional signalling. Nature **378**: 62–65.

van den Berg, C., Willemsen, V., Hendriks, G., Weisbeek, P., and Scheres, B. (1997). Short-range control of cell differentiation in the Arabidopsis root meristem. Nature **390**: 287–289.

Bertolotti, G., Unterholzner, S.J., Scintu, D., Salvi, E., Svolacchia, N., Di Mambro, R., Ruta, V., Linhares Scaglia, F., Vittorioso, P., Sabatini, S., Costantino, P., and Dello Ioio, R. (2021). A PHABULOSA-Controlled genetic pathway regulates ground tissue patterning in the Arabidopsis root. Curr. Biol. **31**: 420–426.e6.

Campos, R., Goff, J., Rodriguez-Furlan, C., and Van Norman, J.M. (2020). The Arabidopsis receptor kinase IRK is polarized and represses specific cell divisions in roots. Dev. Cell **52**: 183–195.e4.

Cartwright, H.N., Humphries, J.A., and Smith, L.G. (2009). PAN1: a receptor-like protein that promotes polarization of an asymmetric cell division in maize. Science **323**: 649–651.

Cederholm, H.M., Iyer-Pascuzzi, A.S., and Benfey, P.N. (2012). Patterning the primary root in Arabidopsis. Wiley Interdiscip. Rev. Dev. Biol. **1**: 675–691.

Coudert, Y., Périn, C., Courtois, B., Khong, N.G., and Gantet, P. (2010). Genetic control of root development in rice, the model cereal. Trends Plant Sci. **15**: 219–226.

Cui, H. (2016). Middle Cortex Formation in the Root: An Emerging Picture of Integrated Regulatory Mechanisms. Mol. Plant **9**: 771–773.

Cui, H. and Benfey, P.N. (2009). Interplay between SCARECROW, GA and LIKE HETEROCHROMATIN PROTEIN 1 in ground tissue patterning in the Arabidopsis root. Plant Signal. Behav. **58**: 1016–1027.

Di Laurenzio, L., Wysocka-Diller, J., Malamy, J.E., Pysh, L., Helariutta, Y., Freshour, G., Hahn, M.G., Feldmann, K.A., and Benfey, P.N. (1996). The SCARECROW gene regulates an asymmetric cell division that is essential for generating the radial organization of the Arabidopsis root. Cell **86**: 423–433.

Dolan, L., Janmaat, K., Willemsen, V., Linstead, P., Poethig, S., Roberts, K., and Scheres, B. (1993). Cellular organisation of the Arabidopsis thaliana root. Development **119**: 71–84.

Doerner, P. (1998). Root development: quiescent center not so mute after all. Curr. Biol. **8**: R42–4.

Dong, J., MacAlister, C.A., and Bergmann, D.C. (2009). BASL controls asymmetric cell division in Arabidopsis. Cell **137**: 1320–1330.

Eshed, Y., Baum, S.F., Perea, J.V., and Bowman, J.L. (2001). Establishment of polarity in lateral organs of plants. Curr. Biol. **11**: 1251–1260.

Facette, M.R., Park, Y., Sutimantanapi, D., Luo, A., Cartwright, H.N., Yang, B., Bennett, E.J., Sylvester, A.W., and Smith, L.G. (2015). The SCAR/WAVE complex polarizes PAN receptors and promotes division asymmetry in maize. Nature Plants **1**: 1–8.

Facette, M.R., Rasmussen, C.G., and Van Norman, J.M. (2019). A plane choice: coordinating timing and orientation of cell division during plant development. Curr. Opin. Plant Biol. **47**: 47–55.

Gallagher, K.L., Paquette, A.J., Nakajima, K., and Benfey, P.N. (2004). Mechanisms regulating SHORT-ROOT intercellular movement. Curr. Biol. **14**: 1847–1851.

Heidstra, R., Welch, D., and Scheres, B. (2004). Mosaic analyses using marked activation and deletion clones dissect Arabidopsis SCARECROW action in asymmetric cell division. Genes Dev. **18**: 1964–1969.

Helariutta, Y., Fukaki, H., Wysocka-Diller, J., Nakajima, K., Jung, J., Sena, G., Hauser, M.-T., and Benfey, P.N. (2000). The SHORT-ROOT gene controls radial patterning of the Arabidopsis root through radial signaling. Cell **101**: 555–567.

Hodge, A., Berta, G., Doussan, C., Merchan, F., and Crespi, M. (2009). Plant root growth, architecture and function. Plant Soil **321**: 153–187.

Kidner, C., Sundaresan, V., Roberts, K., and Dolan, L. (2000). Clonal analysis of the Arabidopsis root confirms that position, not lineage, determines cell fate. Planta **211**: 191–199.

Koizumi, K., Hayashi, T., Wu, S., and Gallagher, K.L. (2012). The SHORT-ROOT protein acts as a mobile, dose-dependent signal in patterning the ground tissue. Proc. Natl. Acad. Sci. U. S. A. **109**: 13010–13015.

Lee, M.M. and Schiefelbein, J. (1999). WEREWOLF, a MYB-Related Protein in Arabidopsis, Is a Position-Dependent Regulator of Epidermal Cell Patterning. Cell **99**: 473–483.

Lehti-Shiu, M.D. and Shiu, S.-H. (2012). Diversity, classification and function of the plant protein kinase superfamily. Philos. Trans. R. Soc. Lond. B Biol. Sci. **367**: 2619–2639.

Lucas, M. et al. (2011). SHORT-ROOT regulates primary, lateral, and adventitious root development in Arabidopsis. Plant Physiol. **155**: 384–398.

Marhava, P., Hoermayer, L., Yoshida, S., Marhavý, P., Benková, E., and Friml, J. (2019). Re-activation of stem cell pathways for pattern restoration in plant wound healing | Elsevier Enhanced Reader. Cell **177**: 957–969.e13.

Nakajima, K. and Benfey, P.N. (2002). Signaling in and out: control of cell division and differentiation in the shoot and root. Plant Cell **14 Suppl**: S265–76.

Nakajima, K., Sena, G., Nawy, T., and Benfey, P.N. (2001). Intercellular movement of the putative transcription factor SHR in root patterning. Nature **413**: 307–311.

Paquette, A.J. and Benfey, P.N. (2005). Maturation of the ground tissue of the root is regulated by gibberellin and SCARECROW and requires SHORT-ROOT. Plant Physiol. **138**: 636–640.

Pillitteri, L.J., Peterson, K.M., Horst, R.J., and Torii, K.U. (2011). Molecular profiling of stomatal meristemoids reveals new component of asymmetric cell division and commonalities among stem cell populations in Arabidopsis. Plant Cell **23**: 3260–3275.

Rasmussen, C.G. and Bellinger, M. (2018). An overview of plant division-plane orientation. New Phytol. **219**: 505–512.

Rowe, M.H., Dong, J., Weimer, A.K., and Bergmann, D.C. (2019). A plant-specific polarity module establishes cell fate asymmetry in the arabidopsis stomatal lineage. bioRxiv: 614636.

Scheres, B., Di Laurenzio, L., Willemsen, V., Hauser, M.T., Janmaat, K., Weisbeek, P., and Benfey, P.N. (1995). Mutations affecting the radial organisation of the Arabidopsis root display specific defects throughout the embryonic axis. Development **121**: 53–62.

Shiu, S.H. and Bleecker, A.B. (2003). Expansion of the receptor-like kinase/Pelle gene family and receptor-like proteins in Arabidopsis. Plant Physiol. **132**: 530–543.

Shiu, S.-H. and Bleecker, A.B. (2001). Plant receptor-like kinase gene family: diversity, function, and signaling. Sci. STKE **2001**: re22–re22.

Sozzani, R., Cui, H., Moreno-Risueno, M.A., Busch, W., Van Norman, J.M., Vernoux, T., Brady, S.M., Dewitte, W., Murray, J.A.H., and Benfey, P.N. (2010). Spatiotemporal regulation of cell-cycle genes by SHORTROOT links patterning and growth. Nature **466**: 128–132.

Springer, N.M. (2010). Isolation of plant DNA for PCR and genotyping using organic extraction and CTAB. Cold Spring Harb. Protoc. **2010**: db.prot5515.

Van Norman, J.M., Breakfield, N.W., and Benfey, P.N. (2011). Intercellular communication during plant development. Plant Cell **23**: 855–864.

Van Norman, J.M. (2016). Asymmetry and cell polarity in root development. Dev. Biol. **419**: 165–174.

Welch, D., Hassan, H., Blilou, I., Immink, R., Heidstra, R., and Scheres, B. (2007). Arabidopsis JACKDAW and MAGPIE zinc finger proteins delimit asymmetric cell division and stabilize tissue boundaries by restricting SHORT-ROOT action. Genes Dev. **21**: 2196–2204.

Wu, S., O'Lexy, R., Xu, M., Sang, Y., Chen, X., Yu, Q., and Gallagher, K.L. (2016). Symplastic signaling instructs cell division, cell expansion, and cell polarity in the ground tissue of Arabidopsis thaliana roots. Proc. Natl. Acad. Sci. U. S. A. **113**: 11621–11626.

Wysocka-Diller, J.W., Helariutta, Y., Fukaki, H., Malamy, J.E., and Benfey, P.N. (2000). Molecular analysis of SCARECROW function reveals a radial patterning mechanism common to root and shoot. Development **127**: 595–603.

Yoshida, S., van der Schuren, A., van Dop, M., van Galen, L., Saiga, S., Adibi, M., Möller, B., Ten Hove, C.A., Marhavy, P., Smith, R., Friml, J., and Weijers, D. (2019). A SOSEKI-based coordinate system interprets global polarity cues in Arabidopsis. Nat Plants **5**: 160–166.

Zhang, X., Facette, M., Humphries, J.A., Shen, Z., Park, Y., Sutimantanapi, D., Sylvester, A.W., Briggs, S.P., and Smith, L.G. (2012). Identification of PAN2 by quantitative proteomics as a leucine-rich repeat--receptor-like kinase acting upstream of PAN1 to polarize cell division in maize. Plant Cell **24**: 4577–4589.

Zhang, X., Zhou, W., Chen, Q., Fang, M., Zheng, S., Scheres, B., and Li, C. (2018). Mediator subunit MED31 is required for radial patterning of Arabidopsis roots. Proc. Natl. Acad. Sci. U. S. A.

CHAPTER II: Exploring the relationship between IRK and endodermal cell division and IRK protein accumulation in ground tissue mutants

INTRODUCTION

The coordination of cell division and differentiation is critical during organ patterning for multicellular organisms. Plants cells are fixed in their relative positions due to a rigid cell wall, and thus spatial cues are important for cell differentiation with cell division orientation being especially important to determine cell fate and organ structure (van den Berg et al., 1995; Facette et al., 2019; Kidner et al., 2000). To study cell division plane orientation, the Arabidopsis root can be used as a model as the nearly invariant cellular organization of the root allows for straightforward detection of defects in cell division orientation and cell identity (Dolan et al., 1993; Benfey and Scheres, 2000). For example, the root ground tissue (GT) is formed through a specific series of oriented, formative cell divisions. First, the cortex and endodermal initial (CEI) divides anticlinally to generate a CEI daughter (CEID). The CEID then divides periclinally to generate the two cell layers of the GT, namely endodermis to the inside and cortex to the outside. In Arabidopsis, the endodermis can undergo an additional periclinal division, which generates an additional GT cell layer called middle cortex (MC) (Baum et al., 2002; Paquette and Benfey, 2005). Formative cell divisions are critical for root tissue patterning, however how cells regulate the timing and extent of these proliferative divisions in a coordinated manner is not fully understood.

In the root meristem, cell-cell communication has been implicated in the regulation of formative cell divisions and cell fate specification (van den Berg et al., 1995, 1997; Wu et al., 2016), therefore these processes are likely influenced by extrinsic factors. A leucine-rich repeat receptor-like kinase (LRR-RLK) named INFLORESCENCE AND ROOT APICES RECEPTOR KINASE (IRK) was recently identified as a polarly-localized receptor required for patterning in the endodermis (Campos et al., 2020). We found that *irk-1* (Salk_038787) exhibited defects in cell divisions in the endodermis; an additional mutant allele was generated via CRISPR-Cas9 that was named *irk-4*. Upon examination, we found that *irk-4* mutant endodermal cells divided prematurely to form MC compared to WT, and also have additional endodermal longitudinal anticlinal divisions (LADs). Additionally, *irk-4* roots exhibit defects in the stem cell niche likely due to displacement of the CEI from the niche and subsequent replacement via neighboring cells (Campos et al., 2020). These phenotypes indicate that IRK functions to restrict endodermal LAD and periclinal divisions and maintain organization of the stem cell niche.

As *irk* mutants exhibit excess periclinal and LADs in the endodermis when compared to WT, we sought to connect IRK with factors known to be involved in GT periclinal cell divisions. A D-type cyclin, *CYCLIN D6;1* (*CYCD6;1*) coincided with the onset of formative cell divisions in the GT (Sozzani et al., 2010), therefore we examined *CYCD6;1* expression for misregulation in *irk*. In WT, the *CYCD6;1* promoter (*pCYCD6;1*) is active in the CEI/CEID and in *cycd6;1* mutants periclinal CEID divisions occur less frequently, indicating that while CYCD6;1 is not necessary for these divisions to occur, it is needed for normal development of the GT. Furthermore, MC divisions were reduced in

cycd6;1, with 52% of roots in WT having MC as compared to only 12% in *cycd6;1* (Sozzani et al., 2010).

Through examination of an IRK-GFP fusion under *pIRK* (*pIRK:IRK:GFP*) we determined that IRK predominantly accumulated in the CEI, CEID, endodermis, and pericycle. Through examination of both endogenous and cell-specific expression of IRK-GFP, we determined that IRK-GFP showed different accumulation patterns across different root cell types. As in the endodermis and pericycle, IRK-GFP localized towards the outer polar domain, and to the inner polar domain when misexpressed in the cortex and epidermis. Furthermore, IRK-GFP localized to the rootward/shootward domains in the CEI and CEID, while in middle cortex IRK-GFP appeared non-polar (Campos et al., 2020). These findings indicate that IRK has specific localization in distinct cell types suggesting its localization depends on the identity of the cells in which it is being expressed.

Lastly, because *irk* mutants have early periclinal divisions in the endodermis, we predict that IRK restricts the timing of endodermal periclinal divisions. Based on these data we sought to identify if *IRK* expression was decreased prior to an endodermal periclinal division. However, in WT only a few endodermal cells at any given time are preparing to undergo periclinal cell division, therefore measurement of *IRK* transcripts in whole roots or root tips may not be sensitive enough to detect a change in expression prior to these divisions. To address this, we proposed that measuring expression of *pIRK:erGFP* prior to this division could detect a change in *pIRK* expression prior to the endodermal periclinal division.

RESULTS

Examining transcriptional regulation of *IRK* during MC development

Microarray data from a SHR induction study identified *IRK* as a putative direct downstream target (Sozzani et al., 2010). Additionally, SHR accumulation decreases prior to periclinal endodermal divisions that generate MC (Koizumi et al., 2012). If, in WT, IRK is a direct downstream target of SHR inducing its expression and, SHR-induced transcription is the primary driver of IRK accumulation at the PM, we predict we would see a decrease in *IRK* promoter activity prior to periclinal endodermal divisions. This hypothesis is supported by our data suggesting that IRK functions to repress these divisions, as in *irk* mutants both periclinal and longitudinal anticlinal endodermal divisions are present in excess.

To determine whether *pIRK* activity levels were reduced prior to periclinal endodermal division, roots expressing *pIRK:erGFP* were imaged at 9 dps on 0.2x MS media (Figure 2.1), which promotes MC formation. erGFP intensity was measured in endodermal cells shootward and rootward of those that had recently undergone periclinal cell division. These measurements were then compared to erGFP intensity in endodermal cells proximal to the QC, which generally do not divide to form MC. We observed that there was no significant difference between *pIRK* activity in endodermal cells adjacent to those that had recently divided periclinally and those that were proximal to the QC. This suggests *pIRK* activity is relatively unchanged in the endodermis prior to MC formation and that down-regulation of *pIRK* is not required for MC formation.

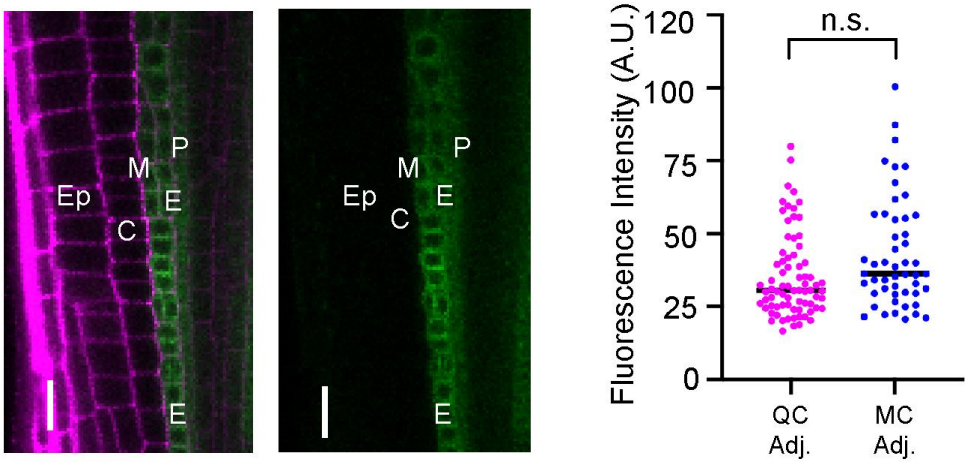

Figure 2.1 Expression of *pIRK*:*erGFP* is unchanged in the endodermis prior to dividing periclinally to generate MC.

Confocal micrographs of a root expressing *pIRK:erGFP* with (A) merged (PI + GFP) and (B) GFP alone, showing expression of *pIRK:erGFP* in the endodermis, middle cortex, and pericycle. (C) erGFP signal (Fluorescence Intensity) is increased but not significantly different in cells adjacent to recently divided endodermis (Blue, MC Adjacent) compared to endodermal cells closer to the QC (Magenta, QC Adjacent). Colored dots represent individual intensity measurements across a cell. Abbreviations: (Ep) Epidermis, (C) Cortex, (M) Middle Cortex, (E) Endodermis, (P) Pericycle. Scale Bar: 25μm. Intensity data collected from 2 individual roots at 9 dps plated on 0.2X MS media with data combined for each region measured. (n.s.) no significance, Student's t-test.

Alternatively, erGFP may be stable in the endoplasmic reticulum and it is not subject to the same post-translational regulation as an endogenous plant protein would be (Snapp, 2009). Thus, it is possible that our measurement of erGFP fluorescence intensity is an inaccurate representation of *pIRK* prior to and during periclinal endodermal divisions.

IRK localization is informed by positional cues not cell identity

IRK localizes to distinct polar domains in different cell types, suggesting IRK polarity is informed by intrinsic cues specific to the cell in which IRK is expressed. To determine if cell identity was sufficient for IRK polar localization in the ground tissue, we expressed *pCO2:IRK:GFP* in *short root* (*shr*) and *scarecrow* (*scr*) mutants, which have defects in GT patterning and cell fate specification. Specifically, *shr* mutants have a single layer of GT with cortex identity based on reporter expression (Figure 2.2A) and the absence of detectable endodermal features (Scheres et al., 1995; Helariutta et al., 2000; Nakajima et al., 2001). *scr* mutants also have a single GT layer, however, this layer is described as having mutant or mixed cell identity as it expresses cortex-specific reporters and exhibits endodermal features, such as periclinal cell division to produce another GT layer (Figure 2.2C) (Scheres et al., 1995; Di Laurenzio et al., 1996; Wysocka-Diller et al., 2000; Paquette and Benfey, 2005). If cell identity alone is sufficient to direct IRK-GFP to specific plasma membrane (PM) domains, then we predict that in *shr*, it would localize to the inner PM domain of the single GT layer (with cortex identity), as it does in WT cortex cells. Furthermore, in *scr*, we predict that localization of IRK would be distinct from *shr* and WT because of the mixed identity of this single GT cell layer.

Upon expression of *pCO2:IRK:GFP* in the *shr* GT, IRK-GFP localized to the shootward and/or rootward PM domains (Figure 2.2B, inset) with accumulation towards the center of these domains (Figure 2.2B and E). Unexpectedly, in the single GT layer of *scr* roots, IRK-GFP also localized to the center of the rootward and/or shootward PM domains (Figures 2.1D). This suggests IRK polarity is not informed by cell identity alone. Interestingly, IRK-GFP localization in single GT layers of *shr* and *scr* roots is similar to that observed in the CEI and CEID of WT roots, which was also a single GT layer. Thus, altogether, our results suggest that localization of IRK in the GT is informed by adjacent cells and may be related to how many GT cell layers there are. These data support a hypothesis whereby positional information, particularly from immediately adjacent cells, directs IRK polar localization in GT cell types.

In the course of these experiments, we observed that IRK-GFP appeared more evenly distributed across some PMs than others. In particular, it appears that in PMs formed during recent transverse anticlinal cell divisions, as determined by relative size of adjacent cells in a file (Figure 2.2D, yellow arrowheads, inset), IRK-GFP is more evenly distributed. This suggests that IRK localization is refined towards the center of cells over time. We also observed that in GT cells immediately adjacent to the (presumed) QC, IRK-GFP was detectable only at the shootward PM domain (Figures 2.2B, asterisks), whereas localization appeared to be at both the rootward and shootward PM domains in GT cells distal of the QC. In summary, we find that in several genotypes IRK localizes at

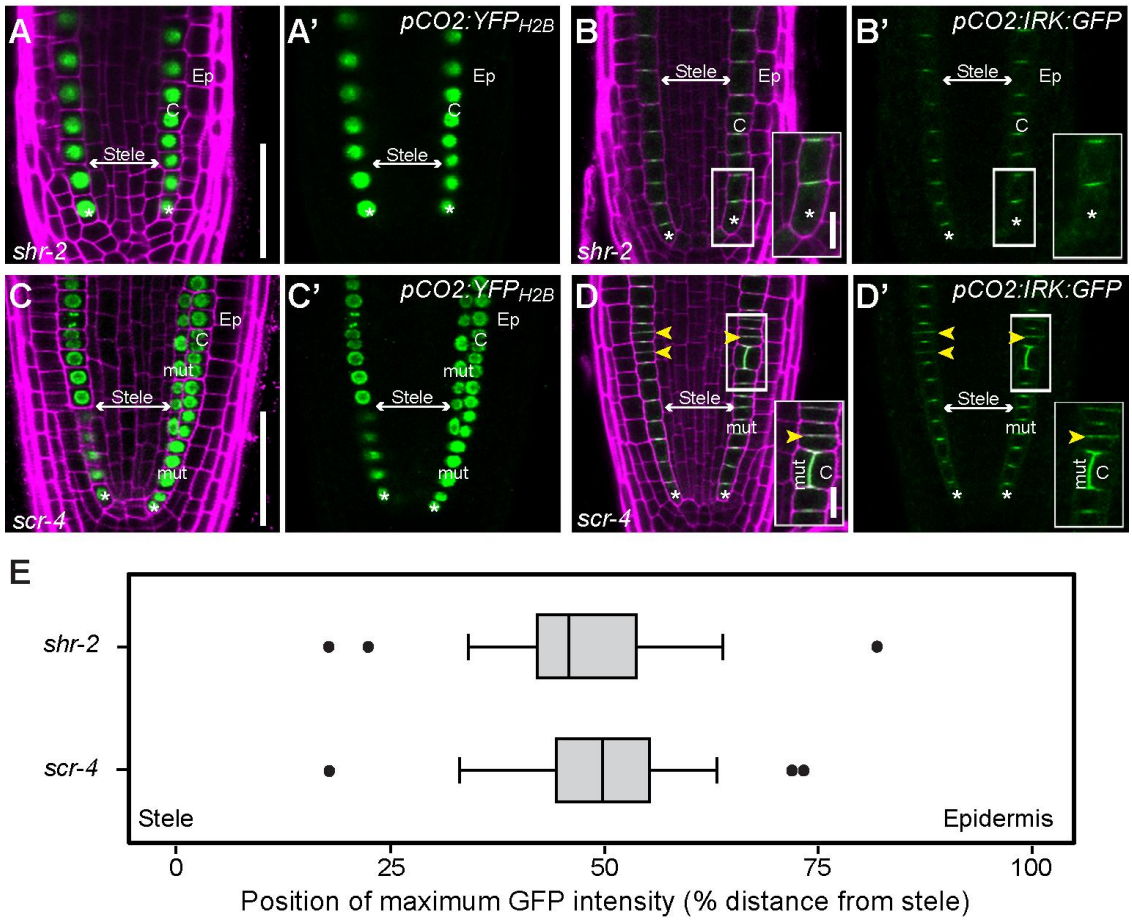

Figure 2.2 IRK localization is not dependent on cell identity.

(A-D) Confocal images of roots expressing fluorescent proteins (FP, green), and stained with propidium iodide (PI, magenta). Adjacent panels show FP + PI merged (A-D) and FP alone (A'-D'). (A) *shr-2* expressing *pCO2:YFP*$_{H2B}$ and (B) *shr-2* expressing *pCO2:IRK:GFP* (5dps). (C) *scr-4* expressing *pCO2:YFP*$_{H2B}$ and (D) *scr-4* expressing *pCO2:IRK:GFP* (7dps). (E) Boxplot showing the position of maximum GFP intensity in single GT layers. Data from a single biological replicate (of three, n = 6 roots per genotype, 5–8 cells per root). Boxes represent the first and third quartiles, median values are marked by the bold line, whiskers indicate 1.5x the interquartile range, and circles indicate outliers. Scale bars: 10 μm in insets of (B) and (D), and 50 μm in all others. Yellow arrowheads in (D, D') indicate recently formed PM due to transverse anticlinal cell divisions. Abbreviations: C, cortex; mut, mutant layer; CEI, cortex/endodermal initial; E, endodermis. Asterisks (*) mark GT cells adjacent to the (putative) QC.

the rootward and/or shootward polar domains when expressed in GT cell types that are present as a single layer.

Consistent with GT cell layer number informing IRK localization, following the periclinal cell division in the single GT layer in *scr*, IRK-GFP becomes laterally polarized (Figure 2.2D, inset). As *pCO2* is active in both of the *scr* GT cell layers (Figure 2.2C) (Paquette and Benfey, 2005), our observations are consistent with IRK-GFP accumulation to the inner PM domain of the outermost GT cell layer (likely cortical cell identity) and outer PM domain of the inner GT cell layer (with mutant or mixed cell identity) (Figure 2.2D). These results suggest that lateral polarity of IRK-GFP is only established when two GT cell layers are present. Our results also show that despite the distinct cell identities of single GT layers in *scr*, *shr,* and WT GT stem cells, IRK-GFP localization is similar, accumulating toward the center of the rootward and/or shootward PM domains. These results indicate that cell identity alone is not sufficient to determine IRK polar localization and, instead, suggests that IRK localization is influenced by extrinsic cues likely from radially adjacent cells.

pCYCD6;1 is misexpressed in *irk* mutants

The *CYCD6;1* promoter (*pCYCD6;1*) is active during formative cell divisions of GT initial and endodermal cells, and is not expressed during proliferative (transverse anticlinal) endodermal divisions (Sozzani et al., 2010). Because our mutant analysis indicates that IRK functions to repress cell divisions in the endodermis, we tested if *CYCD6;1* was misregulated in *irk* mutants. To examine this we crossed *irk-1* and *irk-4* mutants with plants expressing a *CYCD6;1* transcriptional reporter (*pCYCD6;1:erGFP)*.

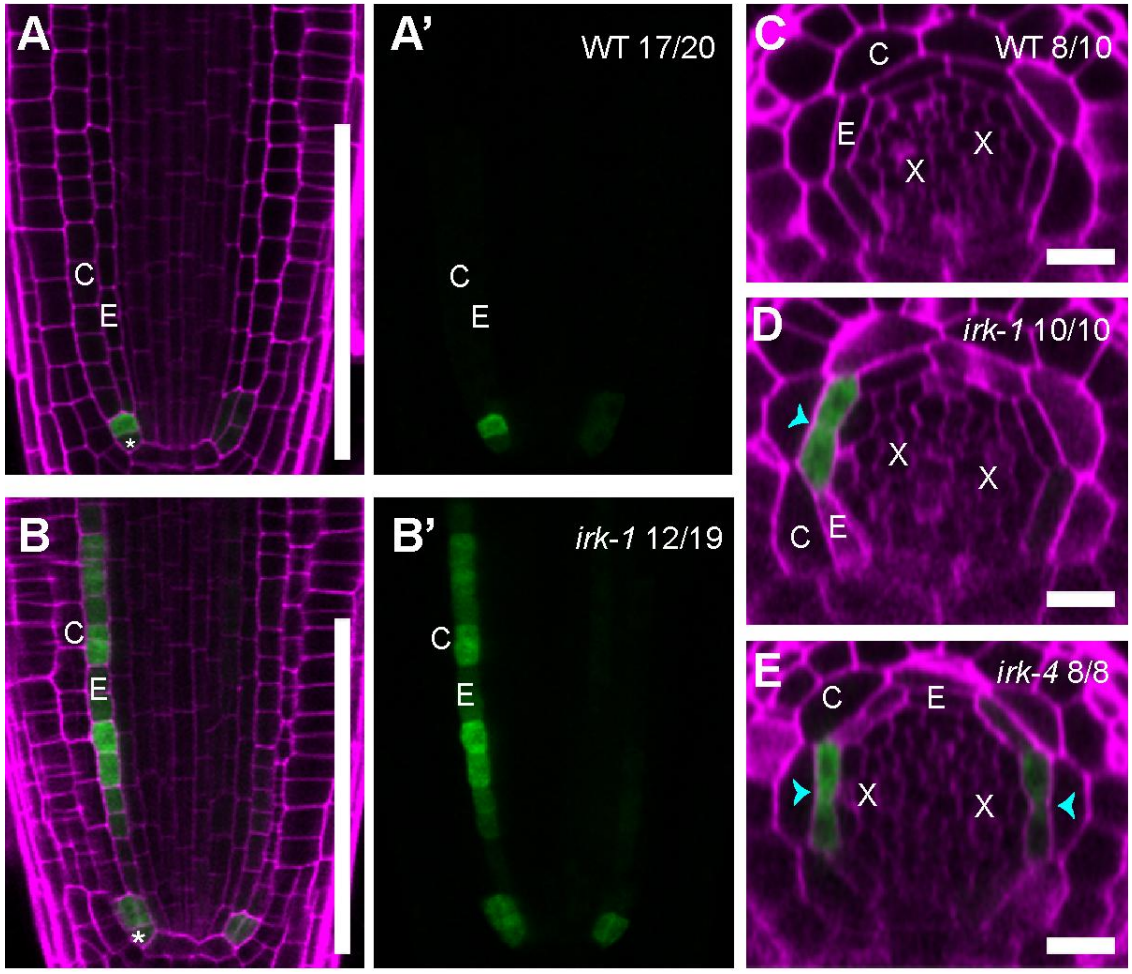

Figure 2.3 Misexpression of *pCYCD6;1* in *irk* mutants.

(A - D) Confocal micrograph showing merged (GFP + PI) and (A', B') GFP alone. (A) Col-0 and (B) *irk-1* roots expressing *pCYCD6;1:GUS:GFP* roots at 5 dps. Number in upper right of (A', B') showing number of roots with the indicated expression pattern out of the total number of roots examined. (C - E) Transverse optical sections at 60µm shootward from the QC with numbers in top right showing number of individual roots showing a similar expression pattern out of total number of roots examined per replicate. Abbreviations: (C) Cortex, (E) endodermis, (X) xylem cells, (asterisk) CEI. Cyan arrows indicate endodermal longitudinal anticlinal division. Scale bars: (A, B) 100µm and (C - E) 20µm.

At 5 dps, *pCYCD6;1* activity is largely restricted to the CEI and CEID in WT, however in *irk-1*, *pCYCD6;1* activity extends shootward in endodermal cell files in the absence of middle cortex formation (Figure 2.3B). Additionally, in the radial axis of WT roots, *pCYCD6;1* activity was rarely observed above the QC, however in *irk-1* and *irk-4*, *pCYCD6;1* activity frequently coincided with endodermal LADs (Figure 2.3C - E).

Therefore, *pCYCD6;1* activity outside the stem cell niche coincides with both periclinal and longitudinal anticlinal endodermal cell divisions in *irk*, suggesting that these cell divisions share a common regulatory mechanism that involves *CYCD6;1* promoter activity and is impinged upon by IRK. We propose that signaling downstream of IRK negatively regulates *CYCD6;1* expression leading to repression of periclinal and longitudinal anticlinal endodermal cell divisions.

DISCUSSION

To further understand the function of IRK during ground tissue development, we need to understand the requirements for IRK localization and expression in the GT connecting IRK function with known regulators of GT development. Polar localization of IRK to distinct PM domains in different cell types is uncommon for an Arabidopsis transmembrane receptor, however it is unclear whether this localization is based on intrinsic or extrinsic cues. Localization of IRK-GFP to the rootward/shootward domain in the single layer of *shr* and *scr* mutants shows that cell identity alone is not sufficient for localization of IRK to the lateral PM domains, and instead suggests that radial cell position within the root meristem informs IRK polar localization. This is evident in *scr* mutants, as when the single layer of GT divides periclinally and the cell adjacent to the

epidermis has cortex identity and the cell adjacent to the pericycle has mixed identity of cortex/endodermis; yet despite this, IRK-GFP localizes to lateral polar domains similar to WT endodermal and cortex cells.

We show that *pCYCD6;1* is more active in *irk* mutant endodermal cells than WT and that it is associated with periclinal and longitudinal anticlinal endodermal divisions in *irk* roots that have not yet formed middle cortex. We propose that *CYCD6;1* expression is downstream of IRK-mediated signal transduction, and that IRK mediated negative regulation of *CYCD6;1* represses periclinal and longitudinal anticlinal endodermal cell divisions.

As there was no significant difference when measuring *pIRK*:*erGFP* in the endodermis prior to a periclinal division, it is still unclear how or if *pIRK* activity is an important factor in regulation of IRK protein level. Because *pIRK* activity is restricted to the meristematic zone in the root, while endodermal accumulation of SHR persists into the differentiation zone (Lucas et al., 2011), it is possible that SHR accumulation decreases in the endodermis prior to periclinal division, but that change may not affect *IRK* promoter activity. Alternatively, it is possible that since erGFP levels were used as a proxy for *IRK* promoter activity that we did not detect changes due to erGFP stability. Furthermore, *IRK* expression may not be solely regulated by SHR and may therefore be unaffected by a decrease in SHR accumulation prior to MC formation. However, given that *irk* mutants show precocious middle cortex formation, a decrease in IRK accumulation would coincide with its proposed function to repress these divisions in the

root meristem. Future work examining *pIRK* expression or IRK protein levels specifically could yield a more clear answer to our question.

EXPERIMENTAL PROCEDURES

Plant materials and growth conditions

Seeds were surface sterilized with chlorine gas, then plated on media (pH 5.7) containing 1% (BD Difco™) Agar and 0.5g/L MES (EMD), supplemented with 1% sucrose w/v and 1x or 0.2x (as indicated) Murashige and Skoog (MS, Caisson labs) basal salts. Plates were sealed with parafilm and stratified on plates in the dark at 4^{o}C for 48-72 hours and then placed vertically in a Percival growth chamber, with 16h light/8h dark cycle at a constant temperature of 22^{o}C.

Confocal microscopy and analysis of fluorescent reporters

Roots were stained with ~10 μM propidium iodide (PI) solubilized in water for 1-2 min and visualized via laser scanning confocal microscopy on a Leica SP8 upright microscope housed in the Van Norman lab. Fluorescence signals were visualized as follows: GFP (excitation 488 nm, emission 492-530 nm), and PI (excitation 536 nm, emission 585-660 nm). All confocal images are either median longitudinal optical sections, transverse optical sections, or part of a Z-stack acquired in the root meristematic zone.

Analysis of IRK localization in GT mutants

scr-4 and *shr-2* mutant seedlings expressing *pCO2:IRK:GFP* were generated

by crossing plants expressing *pCO2:IRK:GFP* with either *scr-4* or *shr-2* then chosen by visually inspecting root morphology prior to visualization via confocal microscopy. Median longitudinal sections of *shr-2* and *scr-4* roots expressing *pCO2:IRK:GFP* were obtained, and GFP intensity across the shootward plasma membrane was measured by using Leica (LAS X) quantification software by generating a line originating at the edge of the GT cell adjacent to the stele and ending at the epidermal edge. The distance from the stele to the epidermis was measured and normalized as a percentage of total distance measured, then the location of maximum GFP intensity was recorded in three biological replicates with similar results in each replicate with 6–10 mutant roots per replicate and GFP intensity was measured in 6–8 cells per root.

Examination of *pCYCD6;1* activity in *irk* mutants

Plants expressing *pCYCD6;1:GUS:GFP* were crossed with *irk-4* and *irk-1* plants independently, then the roots of plants homozygous for either *irk-4* or *irk-1* and *pCYCD6;1:GUS:GFP* were examined at 4, 5 and 7 dps, and roots were scored as positive or negative for GFP fluorescence in the endodermis. In all cases the data shown are from a single biological replicate (of at least three) and similar results were obtained from each biological replicate. Images were analyzed using software accompanying each microscope and assembled into figures in Photoshop (Adobe).

Figure construction

For use in figures, raw confocal images were converted to .TIF format using Leica software (LASX) and were assembled in Adobe Photoshop. Figures containing images and schematics were assembled in Adobe Illustrator.

REFERENCES

Baum, S.F., Dubrovsky, J.G., and Rost, T.L. (2002). Apical organization and maturation of the cortex and vascular cylinder in Arabidopsis thaliana (Brassicaceae) roots. Am. J. Bot. **89**: 908–920.

Benfey, P.N. and Scheres, B. (2000). Root development. Curr. Biol. **10**: R813–5.

van den Berg, C., Willemsen, V., Hage, W., Weisbeek, P., and Scheres, B. (1995). Cell fate in the Arabidopsis root meristem determined by directional signalling. Nature **378**: 62–65.

van den Berg, C., Willemsen, V., Hendriks, G., Weisbeek, P., and Scheres, B. (1997). Short-range control of cell differentiation in the Arabidopsis root meristem. Nature **390**: 287–289.

Campos, R., Goff, J., Rodriguez-Furlan, C., and Van Norman, J.M. (2020). The Arabidopsis receptor kinase IRK Is polarized and represses specific cell divisions in roots. Dev. Cell **52**: 183–195.e4.

Di Laurenzio, L., Wysocka-Diller, J., Malamy, J.E., Pysh, L., Helariutta, Y., Freshour, G., Hahn, M.G., Feldmann, K.A., and Benfey, P.N. (1996). The SCARECROW gene regulates an asymmetric cell division that is essential for generating the radial organization of the Arabidopsis root. Cell **86**: 423–433.

Dolan, L., Janmaat, K., Willemsen, V., Linstead, P., Poethig, S., Roberts, K., and Scheres, B. (1993). Cellular organisation of the Arabidopsis thaliana root. Development **119**: 71–84.

Facette, M.R., Rasmussen, C.G., and Van Norman, J.M. (2019). A plane choice: coordinating timing and orientation of cell division during plant development. Curr. Opin. Plant Biol. **47**: 47–55.

Helariutta, Y., Fukaki, H., Wysocka-Diller, J., Nakajima, K., Jung, J., Sena, G., Hauser, M.-T., and Benfey, P.N. (2000). The SHORT-ROOT gene controls radial patterning of the Arabidopsis root through radial signaling. Cell **101**: 555–567.

Kidner, C., Sundaresan, V., Roberts, K., and Dolan, L. (2000). Clonal analysis of the Arabidopsis root confirms that position, not lineage, determines cell fate. Planta **211**: 191–199.

Koizumi, K., Hayashi, T., Wu, S., and Gallagher, K.L. (2012). The SHORT-ROOT protein acts as a mobile, dose-dependent signal in patterning the ground tissue. Proc. Natl. Acad. Sci. U. S. A. **109**: 13010–13015.

Lucas, M. et al. (2011). SHORT-ROOT Regulates primary, lateral, and adventitious root development in Arabidopsis. Plant Physiol. **155**: 384–398.

Nakajima, K., Sena, G., Nawy, T., and Benfey, P.N. (2001). Intercellular movement of the putative transcription factor SHR in root patterning. Nature **413**: 307–311.

Paquette, A.J. and Benfey, P.N. (2005). Maturation of the ground tissue of the root is regulated by gibberellin and SCARECROW and requires SHORT-ROOT. Plant Physiol. **138**: 636–640.

Scheres, B., Di Laurenzio, L., Willemsen, V., Hauser, M.T., Janmaat, K., Weisbeek, P., and Benfey, P.N. (1995). Mutations affecting the radial organisation of the Arabidopsis root display specific defects throughout the embryonic axis. Development **121**: 53–62.

Snapp, E.L. (2009). Fluorescent proteins: a cell biologist's user guide. Trends Cell Biol. **19**: 649–655.

Sozzani, R., Cui, H., Moreno-Risueno, M.A., Busch, W., Van Norman, J.M., Vernoux, T., Brady, S.M., Dewitte, W., Murray, J.A.H., and Benfey, P.N. (2010). Spatiotemporal regulation of cell-cycle genes by SHORTROOT links patterning and growth. Nature **466**: 128–132.

Wu, S., O'Lexy, R., Xu, M., Sang, Y., Chen, X., Yu, Q., and Gallagher, K.L. (2016). Symplastic signaling instructs cell division, cell expansion, and cell polarity in the ground tissue of Arabidopsis thaliana roots. Proc. Natl. Acad. Sci. U. S. A. **113**: 11621–11626.

Wysocka-Diller, J.W., Helariutta, Y., Fukaki, H., Malamy, J.E., and Benfey, P.N. (2000). Molecular analysis of SCARECROW function reveals a radial patterning mechanism common to root and shoot. Development **127**: 595–603.

Chapter III: Polarly localized receptor-like kinases PXC2 and IRK act redundantly during Arabidopsis root development in the radial axis

INTRODUCTION

In plant development, proper orientation of cell divisions relative to the body axis is required for tissue and organ patterning and overall organ shape (Shao and Dong, 2016; Martinez et al., 2017; Facette et al., 2018; Rasmussen and Bellinger, 2018). Defects in tissue patterning and organ shape can negatively impact organ function (Meyerowitz, 1997; Camilleri et al., 2002). The organization of root tissues and cell types is critical to its function in anchorage and uptake and can be partly attributed to strict regulation of the orientation of cell divisions. In the root, cell divisions are typically oriented periclinally (parallel to the root's surface) or anticlinally (perpendicular to the root's surface) which generates more cells in the radial and/or longitudinal axes respectively. The highly stereotypical organization of root cell types and tissues makes them an ideal model to investigate the mechanisms underlying coordination of oriented cell division and tissue patterning during organ development.

In the Arabidopsis root, the central stele, which contains the pericycle and the vascular tissues, is surrounded by the endodermis, cortex, and epidermis in the transverse axis (Figure 3.1A) (Dolan et al., 1993). In the longitudinal axis, cell types are maintained in linear files that extend from the stem cell niche shootward. For example, in the root ground tissue, the cortex and endodermal cell types are derived from a single stem (initial) cell, the cortex/endodermal initial (CEI). The CEI divides to produce a daughter cell, which then undergoes a periclinal cell division to produce a pair of cell

types: the endodermis towards the inside and the cortex towards the outside (Figure 3.1A) (Dolan et al., 1993; Scheres and Benfey, 1999). Within the root meristem, cells proliferate in longitudinal files extending shootward through transverse anticlinal divisions. In the root ground tissue, longitudinal anticlinal cell divisions rarely occur in the meristem with these divisions producing more ground tissue cells around the stele (Campos et al., 2020). Following proliferation in the meristem, cells undergo dramatic elongation which accounts for the majority of root lengthening (Hodge et al., 2009). In order for the root to maintain its ability to effectively navigate a dynamic and heterogeneous soil environment, precise cellular organization together with coordinated cell elongation must be maintained. Differential cell elongation within the root allows for directional root growth due to positive and negative tropic responses to various aspects of their environment (Correll and Kiss, 2005; Dyson et al., 2014; Dietrich et al., 2017; Su et al., 2017). Thus, disrupting the root's ability to coordinate cell division and/or cell elongation can lead to defects in root form and function.

Coordination of cellular processes, including division and elongation, in any plant organ requires cell-cell communication (Van Norman et al., 2011; Chaiwanon et al., 2016; Wu et al., 2016). Furthermore, orientation of cell divisions and cell fate specification cues are proposed to be based largely on extrinsic factors. This model is supported by cell ablation studies in the root meristem that show altered cell division patterns and cell fate specification when neighboring cells are lost and replaced through division of internal neighbors (van den Burg et al., 1995; van den Berg et al., 1997; Marhava et al., 2019). In plants, members of the large family of receptor-like

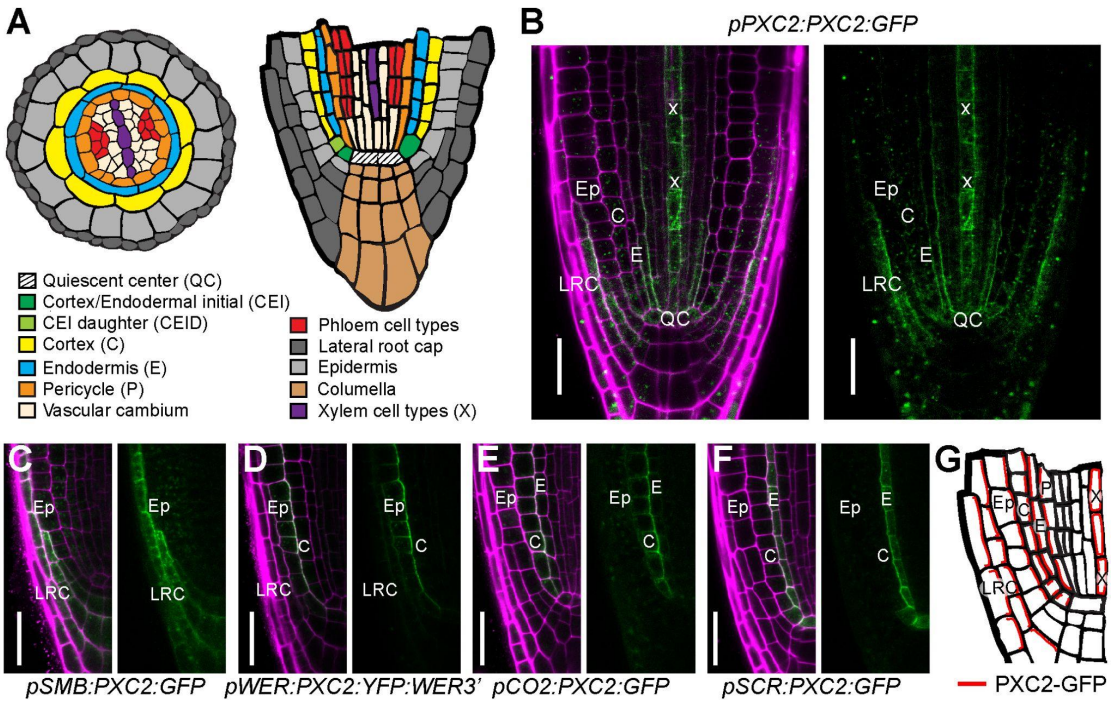

Figure 3.1. PXC2 is polarly localized in root cell types. (A) Schematics of an *Arabidopsis thaliana* root meristem with transverse (left) and longitudinal (right) sections showing cell types and their organization (adapted from (Campos et al., 2020)). (B-G) Confocal micrographs of Arabidopsis root meristems stained with propidium iodide (PI, magenta) to visualize individual cells and showing FP (fluorescent protein) localization (green) with PI + FP (left) and FP alone (right). (B) PXC2-GFP localization when driven by *pPXC2*. (C-F) Polar localization of PXC2-FP upon misexpression by (C) *pSMB*, (D) *pWER*, (E) *pCO2*, and (F) *pSCR*. (G) Schematic summary of PXC2-FP localization inroot cell types. Cell type abbreviations as indicated in (A). Scale bars: 25μm.

kinases (RLKs) are proposed to serve as major participants in intercellular communication across the plant body. The transmembrane group of RLKs contains over 200 members, each with a series of extracellular leucine-rich repeats (LRRs), a single transmembrane domain, and a cytoplasmic kinase domain (Shiu and Bleecker, 2001, 2003). These LRR-RLKs are generally predicted to perceive extracellular ligands and activate downstream signaling pathways. However, many LRR-RLKs remain uncharacterized partially due to high levels of functional redundancy and/or very specific or mild mutant phenotypes (Diévart and Clark, 2003).

The Arabidopsis LRR-RLK, IRK, is polarly localized to the outer (lateral) polar domain in root endodermal cells; yet, in other root cell types, it is localized to distinct domains or is nonpolar (Campos et al., 2020). *irk* mutants have excess longitudinal anticlinal and periclinal endodermal cell divisions and increased stele area in the radial axis. These defects are rescued by expression of IRK from its endogenous promoter or by endodermal-specific expression of IRK, suggesting that abnormal LAD of endodermal cells is the primary defect in *irk* mutants (Campos et al., 2020). Despite the cellular level abnormalities in *irk*, root growth and overall morphology appear largely normal. This led to the question of whether a related LRR-RLK was obscuring a more detrimental dysregulation of endodermal LADs and an enhanced impact on root growth and development.

IRK is most closely related to PXY/TDR-CORRELATED 2 (PXC2, encoded by At5g01890) (Shiu and Bleecker, 2001, 2003; Wang et al., 2013). PXC2 was recently also given the name CANALIZATION-RELATED RECEPTOR-LIKE KINASE (CANAR) and shown to coordinate PIN-FORMED 1 (PIN1) localization during auxin canalization

with *canar* mutants having defects in cotyledon and leaf venation and vascular regeneration after wounding (Hajný et al., 2020). As PXC2 and IRK are both expressed in the root tip (Wang et al., 2013; Campos et al., 2020), we hypothesized that these LRR-RLKs have similar and/or overlapping functions in root development.

Here we show that PXC2 and IRK are present in the same root cell types and, like IRK, PXC2 is localized to the outer (lateral) polar domain in the endodermis and to distinct polar domains or is nonpolar in xylem cells. Unlike *irk* mutants, which show increases in both stele area and endodermal LADs, we find that *pxc2* single mutant roots only show increased stele area. However, *irk pxc2* double mutant roots exhibit a further increase in both endodermal LADs and stele area compared to either single mutant. This indicates that polarly localized IRK and PXC2 function redundantly to repress endodermal LADs and stele area during root development. The double mutant also exhibits an abnormal root growth phenotype that is not present in either single mutant, suggesting enhanced dysregulation of endodermal LADs and stele size negatively impact overall root growth or that IRK and PXC2 are redundantly required for root gravitropism. Finally, we show that misexpressed PXC2 can only partially rescue the *irk* root phenotypes, indicating PXC2 is not functionally equivalent to IRK. We propose these polarized receptors function redundantly in the root in a directional signaling pathway required for coordination of oriented cell divisions, tissue patterning, and growth.

RESULTS

PXC2-GFP is polarly localized root tissues

To examine the expression and localization of PXC2, we generated a transcriptional fusion using the entire intergenic region (4.7 kilobases (kb)) upstream of the *PXC2* start codon (*pPXC2*) to drive expression of endoplasmic reticulum-localized green fluorescent protein (erGFP). In wild-type roots, we observed that *pPXC2* driven erGFP is restricted to the lateral root cap (LRC) and xylem cell types extending shootward from the quiescence center (QC) (Figure 3.2A, B). This is largely consistent with previous examination of *pPXC2* activity via a promoter-driven GUS (β-glucuronidase) reporter (Wang et al., 2013), however, this *pPXC2:GUS* reporter contains just 1.9 kb of the intergenic sequence upstream of *PXC2* ((Wang et al., 2013); Dr. Bo Zhang, personal communication). Thus, differences between these reporters may be due to examination of *pPXC2:erGFP* at higher cellular resolution or to differences in promoter length. These results indicate that *pPXC2* is most active in the LRC and xylem cell types.

To examine PXC2 accumulation, we expressed PXC2 fused to GFP driven by *pPXC2* (*pPXC2:PXC2:GFP*) and observed low levels of the fusion protein in many root cell types with stronger accumulation in the plasma membrane of the LRC and xylem cell types (Figure 3.1B and 3.2C-E). PXC2-GFP was weakly detectable in root cell types beyond where *pPXC2:erGFP* activity was detected (compare Figures 3.1B and 3.2A, D). Like IRK-GFP, the accumulation of PXC2-GFP appeared polarly distributed in the plasma membrane, particularly at the inner polar domain of the outermost layer of the LRC (Figure 3.1B). However, in the xylem cell types, PXC2-GFP appears to have

non-polar accumulation (Figures 3.1B, G and 3.2C). Due to very low GFP signal in most root cell types, it was particularly difficult to determine whether polar accumulation of PXC2-GFP occurred in each cell type.

Despite being driven by the same promoter, our *PXC2* transcriptional and translational reporters show only partially overlapping patterns of expression. Accumulation of the PXC2-GFP fusion protein in cell types beyond those where *pPXC2:erGFP* is detected may be due to very low levels of *pPXC2* activity, which fails to produce enough erGFP for detection. However, when *pPXC2* drives PXC2-GFP expression, this fusion protein may be detectable due to its accumulation at the plasma membrane. Additionally, expression of *pPXC2:PXC2:GFP* rescues the enhanced *irk pxc2* double mutant back to the *irk* single mutant phenotype (see below, Figure 3.6C, D), suggesting the accumulation and function of the *pPXC2:PXC2:GFP* transgene replicates the endogenous situation.

To determine whether PXC2 has similar polar accumulation as IRK, we investigated PXC2-GFP localization upon expression with root cell- or tissue-specific promoters. Because *pPXC2* is highly active in the LRC, we expressed PXC2-GFP from the *SOMBRERO* promoter (*pSMB*), which is expressed specifically in these cells (Willemsen et al., 2008). Expression with *pSMB* confirmed localization of PXC2-GFP to the inner polar domain in the LRC (Figure 3.1C). Additionally, PXC2-GFP expressed

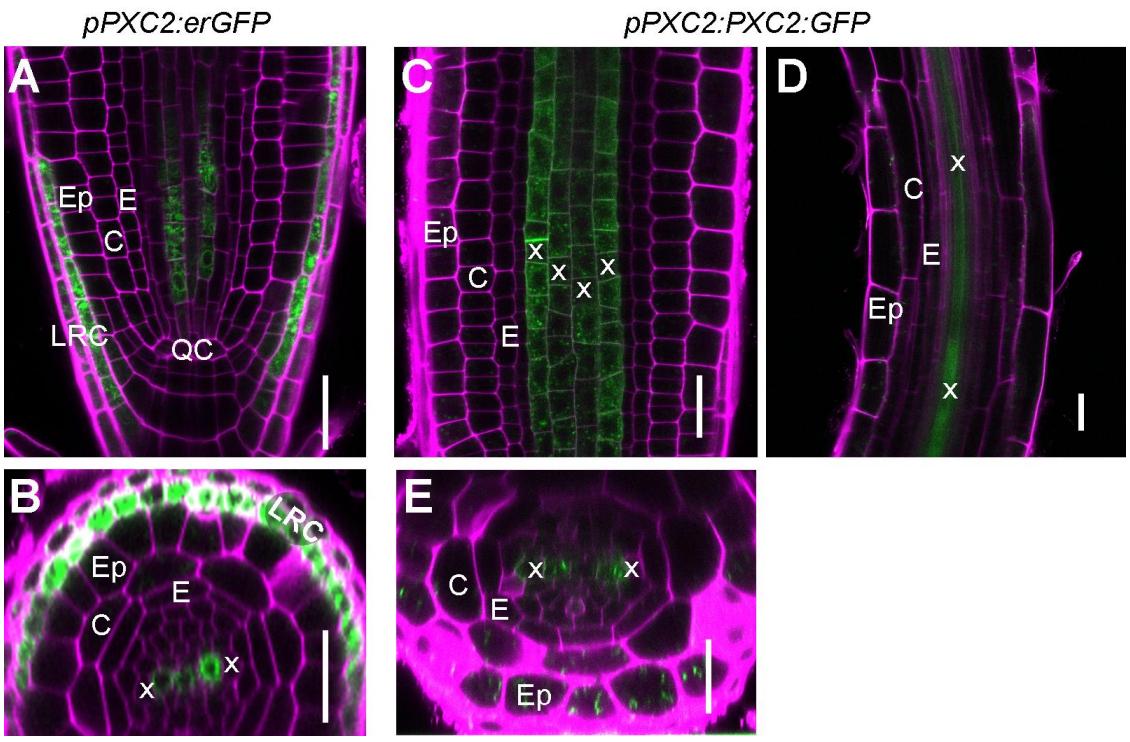

Figure 3.2. *PXC2* promoter activity and PXC2-GFP accumulation across the root developmental zones. (A-E) Confocal micrographs of roots with the propidium iodide (PI) channel (magenta) and GFP channel (green) merged. (A) Median longitudinal and (B) transverse optical sections showing *pPXC2:erGFP* activity in the meristematic zone. (C, D) Median longitudinal sections showing PXC2-GFP accumulation when driven by pPXC2 in xylem cell types in the (C) meristematic and (D) elongation zones. (E) Transverse optical section in the distal root meristem expressing *pPXC2:PXC2:GFP*. Scale bars: 25μm. Abbreviations: (QC) quiescent center, (E) Endodermis, (C) Cortex, (Ep) Epidermis, (LRC) Lateral Root Cap, (x) xylem axis

under control of the *WEREWOLF* promoter (*pWER*) in the LRC and epidermis (Lee and Schiefelbein, 1999) and the *CORTEX2* promoter (*pCO2*) in the cortex (Sabatini et al., 2003; Paquette and Benfey, 2005) was also localized to the inner polar domain (Figure 3.1D, E). Furthermore, similar to IRK, when expressed from *pSCARECROW* (*pSCR*) (Wysocka-Diller et al., 2000), PXC2-GFP localized to the outer polar domain in the endodermis and the rootward/shootward polar domains in the CEI (Figure 3.1F). Cell type/layer-specific expression allowed PXC2-GFP accumulation to be examined without interfering signal from surrounding cells (Alassimone et al., 2010; Campos et al., 2020). Together, these results indicate that, like IRK, PXC2 is a polarly localized LRR-RLK that accumulates to different polar domains in different cell types (Figure 3.1G). The overlapping expression and polar accumulation of IRK and PXC2 are consistent with our hypothesis that they have overlapping or redundant functions in the root.

Mutant alleles of *PXC2* have an enlarged stele area

To study PXC2 function during root development, two insertion alleles were examined, SM_3_31635 (*pxc2-3*) and Salk_055351 (*pxc2-1/canar-1*). We determined that the insertion site in *pxc2-3* resides in the second exon upstream of the sequence encoding the transmembrane domain and generated a premature stop 10 codons after the insertion site (Figure 3.3A). *PXC2* transcript accumulation is reduced in *pxc2-3* (Figure 3.3B) and based on the position of the insertion, *pxc2-3* is unlikely to produce functional protein, making it a likely null allele. The insertion in *pxc2-1/canar-1* is also located in the second exon but is downstream of the sequence encoding the transmembrane domain (Figure 3.3A), suggesting a truncated protein could be

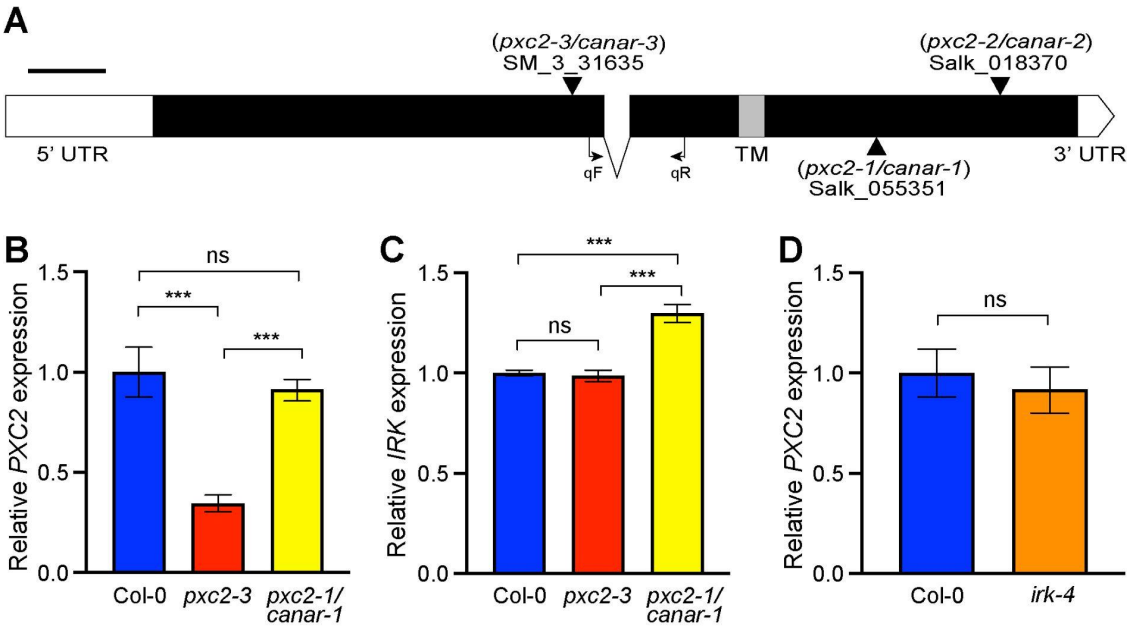

Figure 3.3. *PXC2* gene structure and expression analyses. (A) *PXC2* (At5g01890) gene structure with positions of insertional alleles indicated (triangles), locations of qPCR primers indicated by directional arrows and the region encoding for the transmembrane (TM) domain highlighted in gray. Scale bar: 250 base pairs. (B-D) Expression of *PXC2* and *IRK* relative to controls. (B, C) Col-0, *pxc2-3*, and *pxc2-1*/*canar-1* or (D) Col-0 and *irk-4* samples. Representative data shown from a single biological replicate (of three) with error bars showing standard deviation among three technical replicates. Primers for qRT-PCR on PXC2 are located on either side of the intron and are downstream of *pxc2-3* insertion site. Abbreviations: qF - Forward qPCR primer, qR - Reverse qPCR primer, ns - not significant, *** = p-value <0.001, Student's t-test.

produced. Additionally, we did not find a significant reduction in *PXC2* transcript in *pxc2-1/canar-1* when compared to wild type (Figure 3.3B). The *pxc2-2/canar-2* (Salk_018730) allele was not examined here due to the availability of other alleles that, based on the T-DNA position, we predicted were more likely to be loss of function alleles.

No abnormal root phenotype was detected when *pxc2-3* seedlings were grown on our standard media (not shown), however, when grown on media containing 0.2x Murashige and Skoog (0.2x MS) basal salts, which increases root growth due to lower levels of nitrogen and potassium but does not alter patterning, an abnormal phenotype was observed. Under these conditions, *pxc2-3* roots showed an increase in stele area, but no excess endodermal LADs compared to Col-0 (Figure 3.5A-D). A similar phenotype was also observed in *pxc2-1/canar-1* roots (Figure 3.4A-F), indicating that both alleles disrupt *PXC2* function. These results indicate PXC2 functions to restrict stele area. However, because an abnormal phenotype was detected only on media containing 0.2x MS, PXC2 may serve a relatively minor role in this process, or its role may be dependent on growth conditions. Thus, *pxc2* mutants exhibit a subset of the phenotypes observed in *irk-4* roots, which showed increased stele area and excess endodermal LADs (Campos et al., 2020). Additionally, *IRK* expression is upregulated in the *pxc2-1/canar-1* mutant background, but no significant change in *PXC2* transcript in the *irk-4* mutant was observed (Figure 3.3C, D). These results are consistent with IRK and PXC2 having overlapping or redundant functions in the root.

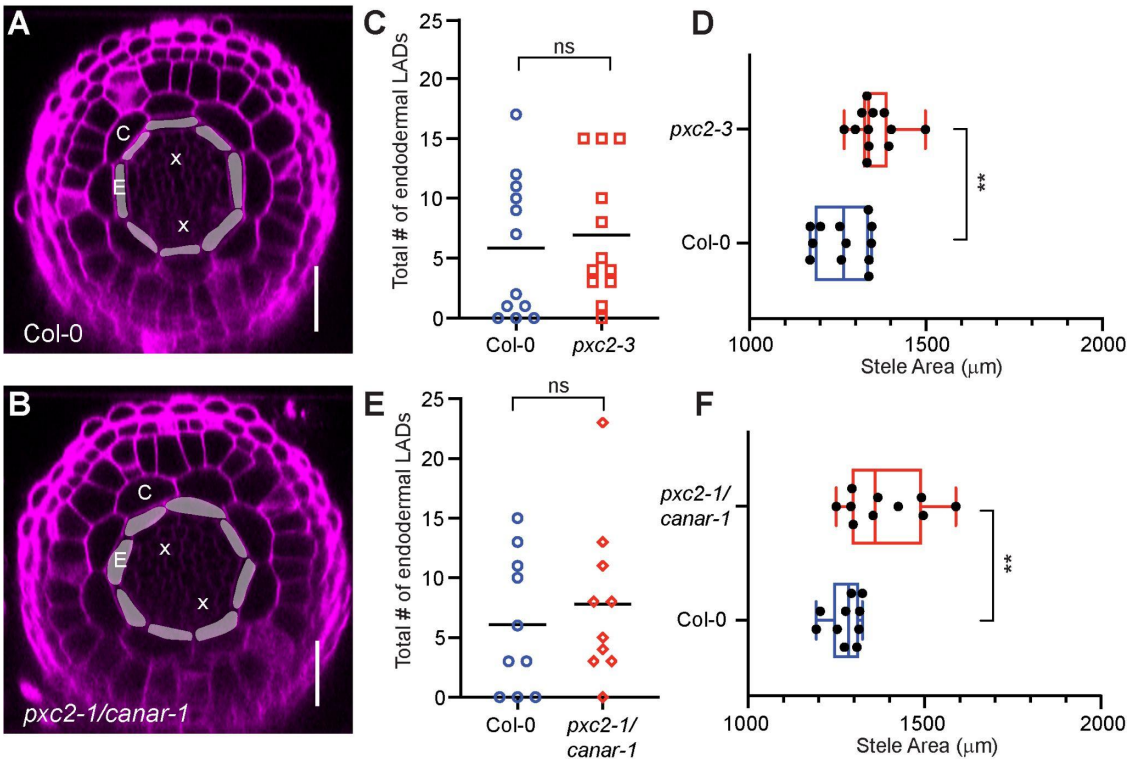

Figure 3.4. *pxc2-3* and *pxc2-1*/*canar-1* roots have similar abnormal root phenotypes. (A, B) Confocal micrographs of transverse sections from root meristems stained with PI (A) Col-0 and (B) *pxc2-1*/*canar-1* at 6 dps with endodermal cells shaded. (C-F) Graphs showing total endodermal LAD and stele area in Col-0 (C, D) and pxc2-3 or (E, F) *pxc2-1*/*canar-1* roots at 6 dps. Data shown from a single representative biological replicate of ≥3 with data in (C, D) shown in Figure 3.5 with rescaled y-axis in (C) for comparison with *pxc2-1*/*canar-1* data. (E, F) n=10 roots per genotype. Scatter plots (C, E): Total number of LADs in individual roots represented by colored symbols with the black bar indicating the mean for each data set. Box plots (D, F): whiskers indicate min/max with interquartile range and mean shown in colored boxes/lines, respectively, and black dots indicate measurements for individual roots. Scale bar: 25μm. Abbreviations: C - cortex, E - endodermis, x - xylem axis, ns = not significant, ** = p value <0.01, Student's t-test.

PXC2 and IRK have redundant functions in restricting stele area and repressing endodermal longitudinal anticlinal cell divisions

To test for functional redundancy, *irk-4 pxc2-3* double mutants were generated by standard genetic crosses. When compared to the single mutants, *irk-4 pxc2-3* roots at 4 dps displayed an enhanced abnormal phenotype with a highly disorganized endodermis, including many additional LADs and further enlargement of stele area (Figure 3.5E-H). Similar to *irk-4*, the excess LADs often occur in endodermal cells adjacent to the xylem pole (Figures 3.5F and 3.6B). At 6 dps, the cell division phenotypes in *irk-4 pxc2-3* roots are substantially more severe (Figure 3.6A, B). This made it difficult to confidently identify whether a cell was the direct product of an endodermal longitudinal anticlinal or periclinal division, consequently, quantification of cell division phenotypes was deemed unreliable in older seedlings. To ensure that the phenotypic enhancement observed in *irk-4 pxc2-3* double mutants was due to simultaneous loss-of-function of both genes and not to disruption at another locus, we expressed the *pPXC2:PXC2:GFP* in the *irk-4 pxc2-3* background and observed rescue of the double mutant phenotype to the level of the *irk-4* single mutant (Figure 3.6C, D). These results indicate that the enhanced *irk pxc2* double mutant phenotype is specific to the simultaneous loss of IRK and PXC2 function.

Enlargement of the stele area in *irk* and *pxc2* single mutants suggests both proteins are required to restrict its size. It is possible that IRK and PXC2 have independent functions in this process, however, they may function redundantly with the lower dosage of gene products in the single mutants leading to weaker phenotypes. Although *pxc2* single mutants do not have excess endodermal LADs, the *irk pxc2*

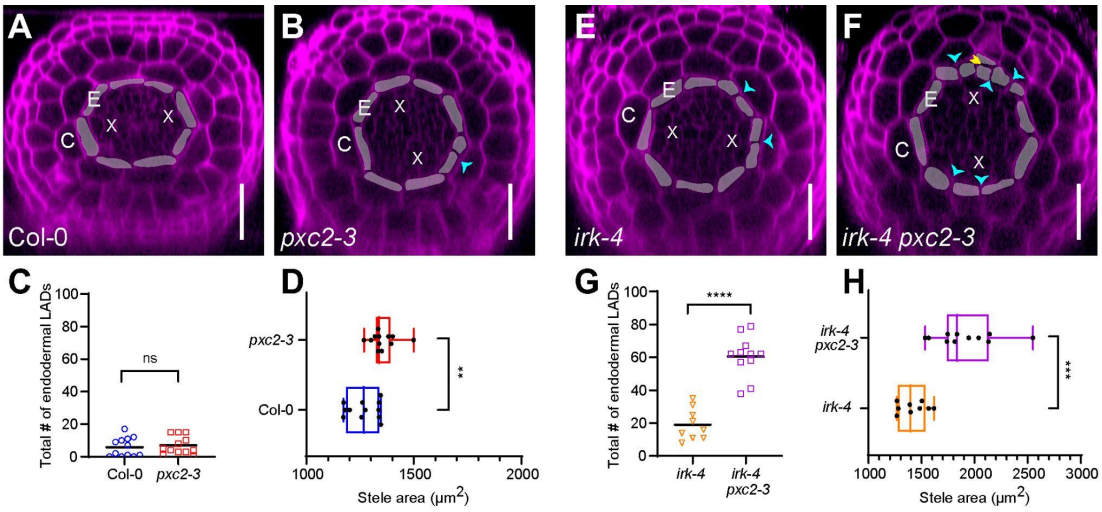

Figure 3.5. Abnormal pxc2 phenotype and enhanced phenotype of irk pxc2 double mutant. (A, B, E, F) Confocal micrographs of Arabidopsis root meristems stained with PI (magenta). (A, B) Transverse optical sections of Col-0 and *pxc2-3* roots at 6 days post stratification (dps). (C, D) Graphs showing total endodermal LADs and stele area in Col-0 and *pxc2-3* at 6 dps (n = 12 roots per genotype). (E, F) Transverse optical sections of *irk-4* and *irk-4 pxc2-3* roots at 4 dps. (G, H) Graphs showing endodermal LADs and stele area in *irk pxc2* double mutants compared to *irk* single mutants (*irk-4* n = 9, *irk-4 pxc2-3* n =11). Data shown are from a single representative biological replicate of ≥3, all with similar results. Scatter plots (C, G): Total number of LADs in individual roots represented by colored symbols with the black bar indicating the mean for each data set. Box plots (D, H): whiskers indicate min/max with interquartile range and mean shown in colored boxes/lines, respectively, and black dots indicate measurements for individual roots. In the micrographs (A, B, E, F), endodermal cells are shaded, cyan arrowheads indicate LADs, and yellow arrowheads indicate periclinal divisions. Scale bar: 25μm. Abbreviations: E - endodermis, C - cortex, x - Xylem, ns = not significant, ** = p value <0.01, *** = p value <0.001, **** = p value <0.0001, Student's t-test.

double mutant has a greater number of these divisions than *irk* alone; thus, we propose that IRK is fully redundant with PXC2 to prevent endodermal LADs. Given the enhanced phenotypic severity in the double mutant, both in terms of endodermal LADs and stele area, we conclude that IRK and PXC2 have redundant functions to negatively regulate these processes.

irk pxc2 double mutants exhibit a root growth defect

While investigating the cellular phenotypes in *irk-4 pxc2-3* roots, we observed a root growth phenotype not present in either single mutant. *irk-4 pxc2-3* roots are somewhat shorter and do not grow as consistently and uniformly downward as wild type, appearing to have a somewhat agravitropic growth phenotype (Figure 3.7B-D). When compared to wild type, *irk pxc2* mutants show reduced root straightness (Figure 3.7A, E), as assessed by the ratio of the distance from hypocotyl to root tip (Dy) divided by total root length. Unlike *irk pxc2* mutants, root length and straightness were not significantly altered in *pxc2-3* and *irk-4* single mutants (Figure 3.6E-H). Furthermore, upon reorientation of the seedlings with respect to the gravity vector, *irk-4 pxc2-3* mutant roots show an attenuated gravitropic response compared to wild type, while the single mutants showed normal responses (Figures 3.7F and 3.6I, J). Additionally, in contrast to WT roots, which exhibit a weak right-slanting (Dx) growth habit (Grabov et al., 2005; Arribas Hernández et al., 2020), all mutant genotypes show a left-slanting growth habit (Figures 3.7A, G I). Because increased stele area and left-slanted growth are observed in each single and in the double mutants, these phenotypes may be related. The agravitropic phenotype and abnormal gravi-stimulation response are unique to *irk pxc2* double mutants but did not impact growth and maturation of these

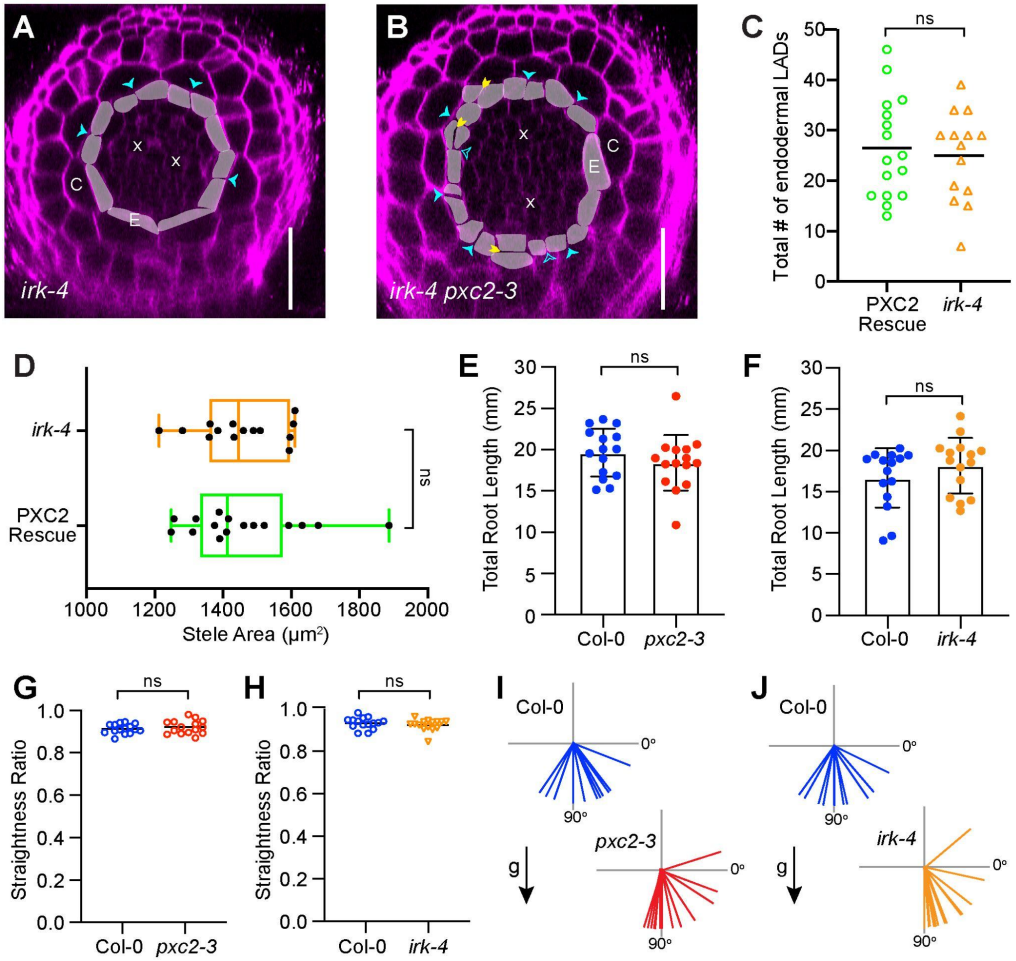

Figure 3.6. Disorganization of *irk-4 pxc2-3* roots is rescued back to *irk-4* by expression of *pPXC2:PXC2:GFP* and *pxc2-3* and *irk-4* single mutant root growth phenotypes. (A, B) Confocal micrographs of transverse optical sections from root meristems stained with PI (A) *irk-4* and (B) *irk-4 pxc2-3* at 6 dps with endodermal cells shaded. Cyan arrowheads indicate LADs, yellow arrowheads indicate periclinal divisions, and cyan outlined arrowheads indicate possible, but uncertain, endodermal LADs based on cell position. Scale bars: 25µm. Note the double mutant phenotype is more severe at 6 dps than 4 dps (compare to Figure 3.5F). (C, D) At 4 dps, expression of *pPXC2:PXC2:GFP* in *irk-4 pxc2-3* (PXC2 Rescue) rescues (C) endodermal LADs and (D) stele area back to the *irk-4* phenotype. (PXC2 Rescue: n = 16, irk-4 n = 14). Data from a single representative biological replicate of ≥3. Box plot (D): whiskers indicate min/max with interquartile range and mean shown in colored boxes/lines, respectively, and black dots indicate measurements for individual roots. Graphs of root growth and phenotypes in Col-0 and *pxc2-3* or *irk-4* roots at 7 dps (E, F) Total root length, (G, H) straightness ratio, and (I, J) Root tip angle 8h after gravistimulation by turning plates 90˚. Colored lines = angle of individual root tips. (E-J) n = 15 per genotype. New gravity vector (90˚) indicated by g and black arrow, previous gravity vector aligned with 0˚. Scatter plots (C, G, H): Data for individual roots indicated by colored symbols with the black bar indicating the mean for each data set. Error bars = standard deviation. All data shown is from a single biological replicate of ≥3. Student's t-test. Abbreviations: C - cortex, E - endodermis, x - xylem axis, ns = not significant.

plants on soil (not shown). These results suggest that enhanced disorganization of root tissues in *irk pxc2* may lead to broader defects in overall root growth or that IRK and PXC2 are redundantly required for normal root gravitropism.

PXC2 is not functionally equivalent to IRK

PXC2 and IRK share 57.1% identity across the entire protein with 65.1% identity between their intracellular domains and have overlapping expression and polar accumulation patterns. *pxc2* mutants exhibit a subset of the *irk* mutant phenotypes and the *irk pxc2* double mutant phenotype is enhanced suggesting functional redundancy. Some related and functionally redundant LRR-RLKs have also been shown to be functionally equivalent when misexpressed. For example, across the entire protein, ERECTA (ER) is 62-63% identical to its functional paralogs ERECTA-LIKE 1 (ERL1) and ERL2 and they are functionally equivalent to ER (Shpak et al., 2004). Similarly, BRI1 and closely related BRI1-LIKE 1 (BRL1) and BRL3, which are 49% identical to BRI1 (Caño-Delgado et al., 2004) and are functionally equivalent to BRI1. Both examples (ERL1/2 and ER, BRL1/3 and BRI1) have comparable amino acid identity as PXC2 and IRK have to each other. Therefore, to further investigate their functional relationship, we examined whether PXC2 was functionally equivalent to IRK.

pSCR-driven misexpression of IRK-GFP was sufficient to rescue the *irk-4* phenotype, including the increase in endodermal LADs and stele area at 60μm above the QC (Campos et al., 2020). Thus, we wanted to determine if *pSCR*-driven expression of PXC2-GFP could similarly rescue the *irk-4* phenotype. In young seedlings (4 dps),

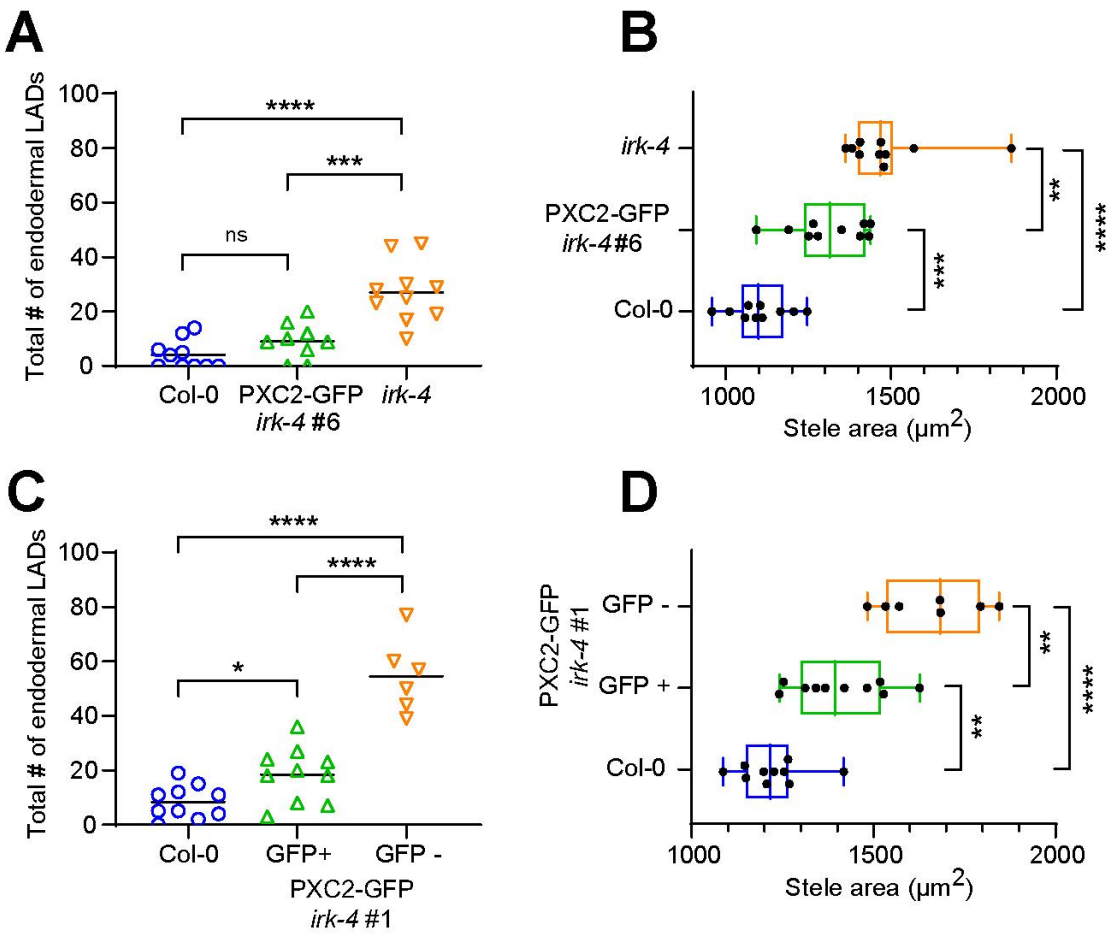

Figure 3.7. *irk pxc2* roots exhibit abnormal growth phenotypes. (A) Schematics of seedlings with different growth phenotypes with measurements indicated for calculating straightness ratio and Dx distance. (B) Col-0 and (C) *irk-4 pxc2-3* seedlings plated on standard media and sealed with tape at 7 dps. Scale bar = 10mm. Graphs of root growth and phenotypes in Col-0 and *irk-4 pxc2-3* roots at 7 dps (D) Total root length, (E) straightness ratio and (G-I) graphs of Dx distance in (G) Col-0 and *pxc2-3* (n = 15 per genotype), (H) Col-0 and *irk-4* (n = 15 per genotype), Col-0 and *irk-4 pxc2-3* (Col-0 n = 14, *irk-4 pxc2-3* n = 13). (F) Root tip angle of Col-0 (top) and *irk-4 pxc2-3* (bottom) roots 8h after gravistimulation by turning plates 90˚. Colored lines = angle of individual root tips. Col-0 (n = 14), *irk-4 pxc2-3* (n = 13). New gravity vector (90˚) indicated by g and black arrow, previous gravity vector aligned with 0˚. Scatter plots (E, G-I): Data for individual roots indicated by colored symbols with the black bar indicating the mean for each data set. Error bars = standard deviation. All data shown is from a single biological replicate of ≥3. n.s = not significant, ** = p value <0.01, *** = p value <0.001, **** = p value <0.0001, Student's t-test.

expression of *pSCR:PXC2:GFP* in *irk-4* rescued the excess endodermal LAD phenotype and, while stele area was significantly reduced compared to *irk-4*, it was not fully rescued (Figure 3.8A, B). Two days later (6 dps), we found only partial rescue of both the endodermal LAD and stele area phenotypes (Figure 3.8C, D). These observations were similar whether the transgene was segregating or was homozygous in *irk-4*. This suggests that increased stele area precedes excess endodermal LADs in *irk-4* roots expressing *pSCR:PXC2:GFP*. Overall, our results indicate that PXC2 is not functionally equivalent to and cannot fully compensate for loss of IRK function.

DISCUSSION

With the characterization of PXC2, we have identified another LRR-RLK involved in polarized cell-cell communication and a new player in cell division regulation that contributes to root patterning, particularly in the radial axis. Similar to IRK, misexpression of PXC2-GFP reveals polar accumulation in various cell types. Their accumulation to distinct polar domains in different cell types suggests localization of IRK and PXC2 is informed by adjacent cells and not organ-level or global polarity cues as proposed for polarly localized nutrient transporters (Alassimone et al., 2010; Takano et al., 2010; Barberon et al., 2014) and the SOSEKI proteins (Yoshida et al., 2019), respectively. Thus, we predict that IRK and PXC2 may share common polarization mechanisms in different cell types.

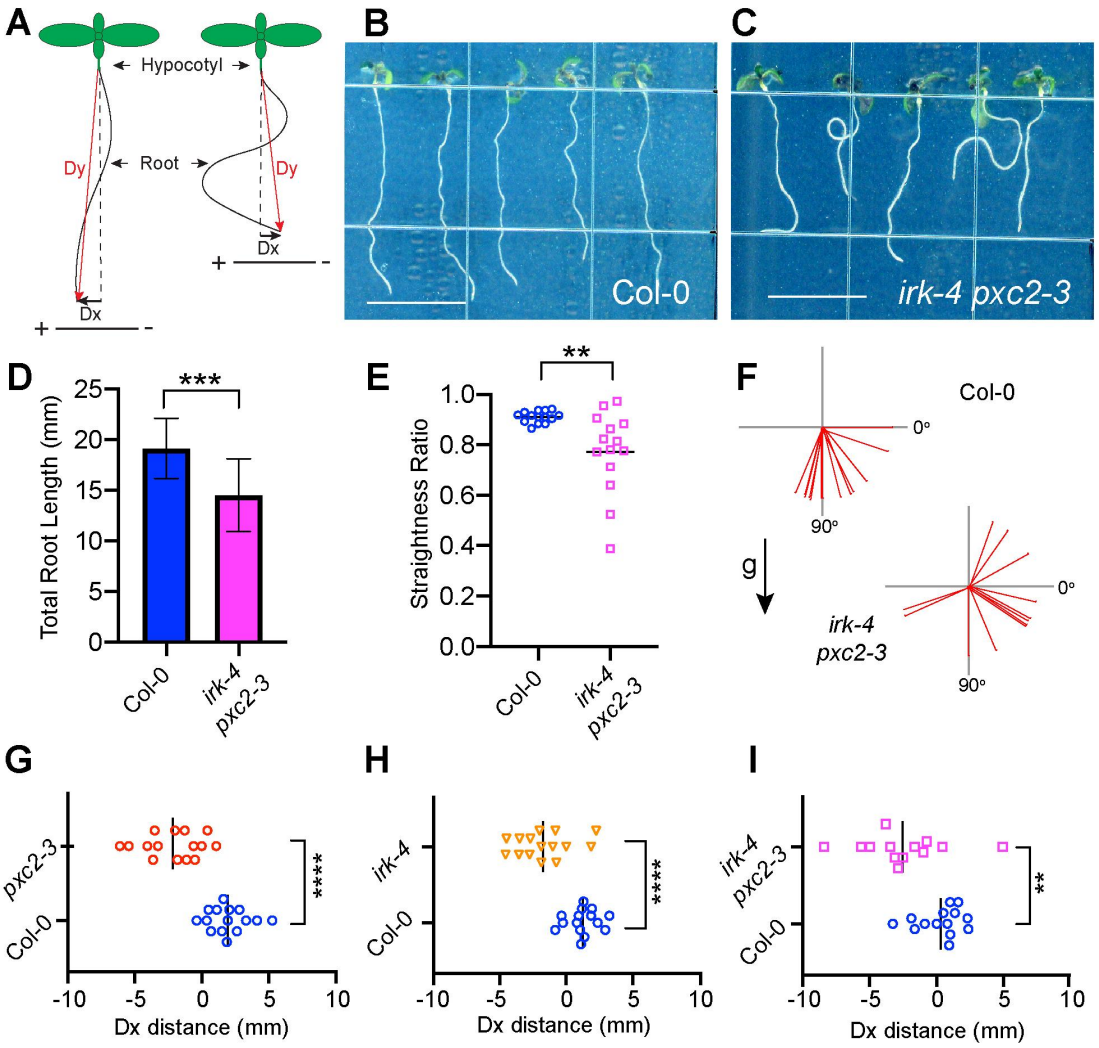

Figure 3.8. PXC2 partially rescues abnormal root phenotypes in *irk*. Graphs showing total number of LADs and stele area in (A, B) Col-0, *irk-4 pSCR:PXC2:GFP*, and *irk-4* plants (at 4 dps, 9-10 roots per genotype) and (C, D) Col-0 and *irk-4* plants segregating for *pSCR:PXC2:GFP* (at 6 dps, Col-0 n = 10, GFP+ n = 10, GFP-, n = 6-7). All data shown are from a single, representative biological replicate of ≥3. Scatter plots (A, C): Total number of LADs in individual roots indicated by colored symbols with the black bar indicating the mean for each data set. Box plots (B, D): whiskers indicate min/max with interquartile range and mean shown in colored boxes/lines, respectively, and black dots indicate measurements for individual roots. Abbreviations: ns = not significant, * = p value <0.05, ** = p value <0.01, *** = p value <0.001, **** = p value <0.0001, Student's t-test.

Examination of *pxc2* mutant roots revealed increased stele area compared to wild type. This phenotype is mild and observed only when seedlings were grown on media containing a lower concentration of MS salts than our standard growth media. This suggests the consequences of loss of PXC2 function are exacerbated by lower nutrient conditions or more rapid root growth. Because IRK and PXC2 are so closely related and the single mutant phenotypes are enhanced in *irk pxc2* double mutants, we conclude that PXC2 and IRK act redundantly to inhibit endodermal LADs and restrict stele area in the root meristem (Figure 3.9A, B). Given the mild abnormal *pxc2* phenotype, our data are consistent with a predominant role for IRK in root development (Figure 3.9B). In wild type, PXC2 and IRK function to limit stele area and repress endodermal LADs, such that there are typically only 8 endodermal cells around the stele (Figure 3.9B, left). In *pxc2* mutants, we observe an increase in stele area while endodermal cell number remains the same as wild type. This indicates that IRK activity alone is sufficient to repress endodermal LADs, but not to fully restrict stele area (Figure 3.9B, center-left). In contrast, in *irk* mutants, increased stele area and endodermal cell number around the stele are observed, indicating PXC2 alone is not sufficient to restrict endodermal LADs and stele area to WT levels (Figure 3.9B, center-right). In the double mutant, enhanced increases in stele area and endodermal LADs indicate PXC2 and IRK function redundantly to restrict them (Figure 3.9B, right); additionally, IRK appears fully redundant to PXC2 in repression of endodermal LADs. However, PXC2 and IRK may not be fully redundant with regard to repression of stele area, as it is enlarged in each single mutant. Alternatively, a lower dosage of these gene products may lead to weaker single mutant phenotypes compared to the double mutant.

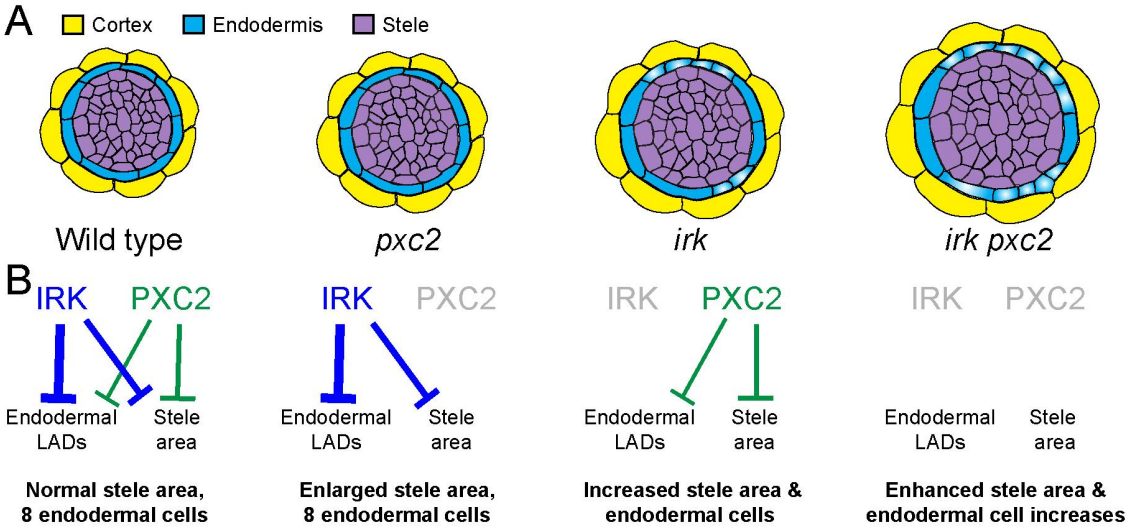

Figure 3.9. Summary of IRK and PXC2 function to restrict stele area and endodermal LADs and phenotypic outcomes. (A) Schematic representations of transverse sections of the root showing phenotypes observed in endodermal cells and stele in Col 0, *pxc2*, *irk*, and *irk pxc2*. Highlighted endodermal cells indicate the occurrence of LADs. (B) Diagrams illustrating the relative roles of IRK and PXC2 in each genotype with regard to restriction of stele area and endodermal LADs. Weight of the lines indicates the proposed contribution of each protein to the processes with the phenotypic outcomes listed below each.

Although we propose they have partially overlapping functions, misexpression of PXC2 is not sufficient to compensate for the loss of IRK. We unexpectedly observed that endodermal-specific expression of PXC2-GFP only rescued the endodermal LAD phenotype in *irk-4* roots. This is in contrast to *pSCR* driven expression of IRK-GFP, which rescues the increased endodermal LADs and stele area phenotypes in *irk-4*. Based on this, we previously concluded that increased stele area was a secondary defect in *irk-4* due to excess endodermal LADs. However, the relationship between endodermal cell number and stele area may be more complicated. For example, in *pxc2* roots (at 6 dps) and *irk-4 pSCR:PXC2:GFP* roots (at 4 dps), we do not observe excess endodermal LADs; yet stele area is enlarged, suggesting an increase in stele area precedes the occurrence of endodermal LADs in these genotypes. This is supported by the observation that *irk-4 pSCR:PXC2:GFP* roots at a later time (6 dps) show an enlarged stele and excess endodermal LADs (Figure 3.7C, D). Thus, it is possible that dysregulation or uncoupling of communication between the endodermis and stele leads to the observed phenotypes, hinting at mechanical feedback between tissues in the root's radial axis. For instance, if excess endodermal LADs broaden the root in the radial axis, stele area may increase as a consequence. On the other hand, if stele area increases, endodermal LADs may occur to accommodate this. Further exploration of the cell type-specific functions of IRK and PXC2 during root development will allow deeper functional insights into these proteins and suggests these proteins can serve as novel tools to dissect the interaction between endogenous genetic control and exogenous mechanical feedback during developmental patterning.

Finally, *irk pxc2* double mutants exhibit an agravitropic root growth phenotype, not observed in either single mutant. This suggests that IRK and PXC2 are redundantly

required for normal root growth. This growth phenotype may be attributed to the large increases in endodermal cell number and stele area in the double mutant, as directional growth requires the coordinated elongation of neighboring cell types (Sablowski, 2016; Vaahtera et al., 2019). For instance, because the endodermal LADs in the mutants tend to occur nonuniformly in the radial axis (Figures 2F and 3.6B, (Campos et al. 2020)), regions with smaller, more numerous endodermal cells could impede coordinated cell expansion. Additionally, the increase in endodermal periclinal cell divisions would result in variable numbers of ground tissue layers in the root's radial axis. Thus, difficulties in coordination of cell elongation across root cell layers that are non-uniform in cell number may give rise to an agravitropic growth phenotype. Alternatively, recent data indicates PXC2/CANAR binds to and coordinates the polarization of PIN1, an auxin efflux carrier, in shoot tissues (Hajný et al., 2020). This suggests another explanation for the *irk pxc2* root growth phenotype as root gravitropism requires the (re)polarization of PINs to achieve differential auxin distribution and cell elongation (Friml et al., 2002; Kleine-Vehn et al., 2010). Therefore, if PXC2 and, by extension, closely related IRK, have similar interactions with PINs in the root, this could explain the agravitropic phenotype of the *pxc2 irk* double mutant and will be an important avenue of future work. Given our collective results, we hypothesize a crucial relationship exists between the polarity and function of PXC2 and IRK and coordinated cell division, radial patterning, and cell elongation during root growth and development.

EXPERIMENTAL PROCEDURES

Plant materials and growth conditions

Seeds were surface sterilized with chlorine gas, then plated on media (pH 5.7) containing 1% (BD Difco™) Agar and 0.5g/L MES (EMD), supplemented with 1% sucrose w/v and 1x Murashige and Skoog (MS, Caisson labs) basal salts (our standard growth medium) or 0.2x MS salts (as noted). Plates were sealed with parafilm or 3M micropore tape as indicated below. Seeds were stratified on plates in the dark at 4°C for 48-72 hours and then placed vertically in a Percival growth chamber, with 16h light/8h dark cycle at a constant temperature of 22°C.

Confocal microscopy and analysis of fluorescent reporters

Roots were stained with ~10 μM propidium iodide (PI) solubilized in water for 1-2 min and visualized via laser scanning confocal microscopy on a Leica SP8 upright microscope housed in the Van Norman lab. Root meristems were visualized in the median longitudinal, transverse planes, or as Z-stacks. Fluorescence signals were visualized as follows: GFP (excitation 488 nm, emission 492-530 nm), YFP (excitation 514 nm, emission 515-550 nm), and PI (excitation 536 nm, emission 585-660 nm). All confocal images are either median longitudinal optical sections, transverse optical sections, or part of a Z-stack acquired in the root meristematic or elongation zone. Images of roots expressing *PXC2* transcriptional or translational

fusions were taken at either 5 or 7 dps with no observable differences due to age. Roots misexpressing PXC2-FP using cell type-specific promoters were imaged at 5 dps.

Endodermal LAD quantification and stele area measurement

All images of roots for analysis of endodermal LADs and stele area were taken as Z stacks at 512x512 resolution with 1µm between scans, speed setting at 600 with a line average of six. Z-compensation was used by increasing 588 nm laser intensity while focusing through the Z plane, from 2% up to 40% (depending on staining) in order to visualize cell layers adjacent to the slide (in the radial axis).

Total number of endodermal LADs were determined by counting the number of endodermal cells per ring of cells in the transverse plane starting from just above the QC. Because cells of the cortex and endodermis are formed as a pair through periclinal division of a single initial cell, endodermal LADs typically result in two or more small endodermal cells adjacent to a single cortex cell. For each individual root, 15 endodermal rings were scored for occurances of LADs, the presence of an additional longitudinal anticlinal wall within a ring of endodermal cells was scored as an LAD and then summed. If any of the first 15 endodermal cells were damaged (PI infiltration) the root was not used in the analysis.

Stele area was measured in the transverse section located 60μm above the QC using ImageJ software. The inner cell wall of the endodermis was traced and used to calculate the area of the region in ImageJ. If the stele was damaged or staining was too weak to accurately determine the endodermal border then that root was excluded from the analysis.

Phenotypic characterization of *pxc2* and *irk-4 pxc2* mutants

pxc2-3/canar-3 (SM_3_31635) and *pxc2-1/canar-1* (Salk_055351) seeds were obtained through the Arabidopsis Biological Research Center and genotyped using primers listed in Table S1 to identify homozygous mutants. Age matched seeds from plants grown for three generations in the lab were used in these studies. Each mutant was plated with Col-0 on individual plates. Seeds were sown on plates containing 0.2x MS media and sealed with paraflim. At 6 dps, Z-stacks were obtained for *pxc2* mutants and Col-0 root tips (n = 10-15 per genotype) for quantification of endodermal LADs and stele area. No additional root cellular morphology phenotype was observed for either *pxc2* mutant.

Standard genetic crosses between *pxc2-3* and *irk-4* plants were completed to generate *irk-4 pxc2-3*. F2 plants were genotyped to identify genotypes of interest and then confirmed in subsequent generations. Double mutant seeds collected from genotyped F3s were used in these studies. *irk-4 pxc2-3* mutants were plated with *irk-4* as the controls on plates containing 1x MS media and sealed with parafilm. At 4 dps, Z-stacks were obtained for *irk-4 pxc2-3* and *irk-4* (n = 10-15 per genotype) for

quantification of endodermal LADs and stele area. Additional imaging was conducted at 6 dps, however, quantification of stele area and endodermal LAD was not performed due to severe defects.

For the root length, straightness ratio, and gravi-stimulation analyses, Col-0, *pxc2-3*, *irk 4*, and *irk-4 pxc2-3* seeds were plated on our standard media and sealed with micropore tape and plates were scanned (EPSON V600) at 7 dps. After scanning, the plates were turned 90^{o} and placed back into the growth chamber for 8 hours, then scanned again. From the first scans, total root length was measured by tracing individual roots from the base of the hypocotyl to the root tip using the segmented line feature in ImageJ. Then, a straight line was drawn from the base of the hypocotyl to the root tip and measured as Dy (Figure 3.8A). The straightness ratio is calculated by dividing Dy by total root length where a ratio of 1.0 indicates root growth always parallel with the gravity vector. To assess Dx (Figure 3.8A), a straight line was first drawn directly downward from the base of the hypocotyl to the region parallel to the root tip. Then, a straight line was drawn from this point to the root tip, resulting in the Dx measurement, with a positive value assigned to the rightward direction of root drift as observed in Col-0. From the second scans (8 hours after gravistimulation), the angle between 1mm of the root tip and the new gravity vector were measured in ImageJ to assess the root's response following gravistimulation.

PXC2-GFP rescue of *irk-4*

irk-4 plants homozygous for *pSCR:PXC2:GFP*, Col-0, and *irk-4* mutants were plated on 1x MS media and imaged at 4 dps as previously described. *irk-4* mutants segregating for *pSCR:PXC2:GFP* and Col-0 were plated together on media previously

described and imaged at 6 dps. Two independent transgenic lines (#4 and #6) were crossed with *irk-4* for analysis at both 4 and 6 dps with similar results.

Vector construction and plant transformation

Transcriptional and translational reporters were constructed by standard molecular biology methods and utilizing Invitrogen Multisite Gateway® technology (Carlsbad, USA). The 4.7 kb region upstream of the *PXC2* (At5g01890) start codon was amplified from Col-0 genomic DNA and recombined into the Invitrogen pENTR™ 5'-TOPO® TA vector as the promoter of *PXC2*. For the transcriptional reporter, *pPXC2* drove endoplasmic reticulum-localized green fluorescent protein (erGFP) as previously described (Van Norman et al., 2014). For translational fusions, the genomic fragment encoding *PXC2* from the ATG up to, but excluding the stop codon (including introns, 3.0 kb), was amplified from Col-0 genomic DNA and recombined into the Invitrogen pENTR™ DIRECTIONAL TOPO® (pENTR-D-TOPO) vector and fused to a C terminal GFP tag as previously described (Van Norman et al., 2014).

Cell type- or layer-specific promoters (*pSCR$_{2.0}$, pCO$_2$,* and *pWER)* as previously described (Campos et al., 2020; Lee et al., 2006), and *pSMB* as described (Bennett et al., 2010) were used to drive PXC2-GFP. The various Gateway compatible fragments were recombined together with the dpGreen-BarT (Lee et al., 2006) or dpGreen-NorfT (Norflurazon resistant) destination vectors. The dpGreenNorfT was generated by combining the backbone of dpGreenBarT with the *p35S::tpCRT1* and terminator insert from *pGII0125*. Within the target region of the dpGreenBarT, one AclI site was mutated with the QuickChangeXL kit (Stratagene). Plasmids were amplified in ccdB-resistant *E. coli* and plasmids prepped with a Bio Basic Plasmid DNA Miniprep kit. 34uL of the

modified dpGreenBarT and unmodified *pGII0125* were digested with 1ul each FspI and AclI in CutSmart buffer (NEB) for 1hr at 37˚C. Digests were subjected to gel electrophoresis on a 1% agarose gel. The 5866bp fragment from the dpGreenBarT and 2592bp fragment from the *pGIII0125* were extracted with a Qiagen MinElute Gel Extraction kit. The fragments were then ligated at 1:1 volumetric ratio (20ng vector; 8.8ng insert) using T4 DNA ligase incubated at 16˚C overnight before transformation into ccdB-resistant *E. coli*.

Expression vectors were then transformed into Agrobacterium strain GV3101 (Koncz et al., 1992) and then into Col-0 plants by the floral dip method (Clough and Bent, 1998). Transformants were identified using standard methods. For each reporter, T2 lines with a 3:1 ratio of resistant:sensitive seedlings, indicating the transgene is inherited as a single locus, were selected for propagation. These T2 plants were allowed to self and among the subsequent T3 progeny, those with 100% resistant seedlings, indicating that the transgene was homozygous, were used in further analyses. For each reporter, at least three independent lines with the similar relative expression levels and localization patterns were selected for imaging by confocal microscopy.

Figure construction

Confocal images for stele area measurement and endodermal LAD quantification were examined in ImageJ (http://imagej.nih.gov/ij) (Schneider et al., 2012). For use in figures, raw confocal images were converted to .TIF format using Leica software (LASX) and were assembled in Adobe Photoshop. Statistical analysis and graphical representation of all data in this publication was done using PRISM8

(GraphPad Software, https://www.graphpad.com/, San Diego, USA). Type of graphs and statistical analysis used are listed in figure legends. Schematics were created in Illustrator and then figures containing images, graphs, and schematics were assembled in Adobe Illustrator.

qRT-PCR analysis

Total RNA was isolated from seedlings at 7 dps of three independent biological replicates for each Col-0 (wild type), SM_3_31635 (*pxc2-3/canar-3*) and Salk_055351 (*pxc2-1/canar-1*) using Qiagen RNeasy Plant Mini Kit. Seeds of all three genotypes were sown together on plates containing 1x MS media, sealed with parafilm, and stratified in the dark at 4˚C for 3 overnights. Following total RNA extraction, samples were examined for concentration and purity and stored at -80˚C prior to cDNA synthesis. For cDNA synthesis (RevertAid First Strand cDNA Synthesis Kit,Thermo Scientific), 1µg of total RNA was used to normalize for varying RNA concentrations within biological samples, and the Oligo(dT)18 primer was used to generate cDNA. To examine *PXC2* expression in *irk-4*, previously obtained RNA samples (Campos et al. 2020) were used. qRT-PCR reactions were done using IQ SYBR Green Supermix (BioRad) and analysis was performed on the CFX Connect Real-Time System housed in the Integrative Institute of Genome Biology Genomics Core facility at UC-Riverside. The reaction conditions for all primer pairs were: 95˚C for 3 min, followed by 40 cycles of 95˚C for 10s and 60˚C for 30s. Primer pair efficiency was calculated for each reaction using standard curve data. For each genotype and biological replicate, three technical

replicates were performed, and all transcript levels were normalized to *PHOSPHATASE 2A* (*PP2A*) (Czechowski et al., 2005). Data analysis was done using Bio-Rad CFX Maestro 1.1 (version 4.1.2433.1219).

Gene structure and amino acid sequence comparisons

DNA sequence of *PXC2* including 5' and 3' UTR was copied into the web-based http://wormweb.org/exonintron tool and annotated with the positions of the T-DNA insertions based on DNA sequencing for *pxc2-3* and using publicly available data from The Arabidopsis Information Resource (TAIR, www.arabidopsis.org) for *pxc2-1/canar-1* and *pxc2-2/canar-2*. Percent identity for PXC2 and IRK and of ERL1 and ERL2 to ER and BRL1 and BRL3 to BRI1 were obtained using the web based Clustal Omega tool (https://www.ebi.ac.uk/Tools/msa/clustalo/).

ACKNOWLEDGMENTS

We thank Roya Campos for assistance in the construction of several PXC2-GFP misexpression vectors and Dr. Dawn Nagel, Dr. Cecilia Rodriguez-Furlan, Roya Campos, and Jessica Toth for discussions of the project and feedback on the manuscript while it was in preparation. We also thank Dr. Erin Sparks (University of Delaware) for providing the NorfT Gateway® compatible destination vector. We appreciate access to and assistance from the Institute of Integrative Genome Biology Genomics Core Facility (UC, Riverside) for qRT-PCR experiments. This work was

supported by funds awarded to JMVN, specifically by Initial Compliment (IC) funds from the University of California at Riverside, USDA-NIFA-CA-R-BPS-5156-H, and by an NSF CAREER award (#1751385).

REFERENCES

Alassimone, J., Naseer, S., and Geldner, N. (2010). A developmental framework for endodermal differentiation and polarity. Proc. Natl. Acad. Sci. U. S. A. **107**: 5214–5219.

Arribas-Hernández, L., Simonini, S., Hansen, M.H., Paredes, E.B., Bressendorff, S., Dong, Y., Østergaard, L., and Brodersen, P. (2020). Recurrent requirement for the m6A ECT2/ECT3/ECT4 axis in the control of cell proliferation during plant organogenesis. Development **147**.

Barberon, M., Dubeaux, G., Kolb, C., Isono, E., Zelazny, E., and Vert, G. (2014). Polarization of IRON-REGULATED TRANSPORTER 1 (IRT1) to the plant-soil interface plays crucial role in metal homeostasis. Proc. Natl. Acad. Sci. U. S. A. **111**: 8293–8298.

Bennett, T., van den Toorn, A., Sanchez-Perez, G.F., Campilho, A., Willemsen, V., Snel, B., and Scheres, B. (2010). SOMBRERO, BEARSKIN1, and BEARSKIN2 regulate root cap maturation in Arabidopsis. Plant Cell **22**: 640–654.

van den Berg, C., Willemsen, V., Hendriks, G., Weisbeek, P., and Scheres, B. (1997). Short range control of cell differentiation in the Arabidopsis root meristem. Nature **390**: 287–289.

van den Burg, C., Willemsen, V., Hage, W., Weisbeek, P., and Scheres, B. (1995). Cell fate in the Arabidopsis root meristem determined by directional signaling. Nature **378**: 62.

Camilleri, C., Azimzadeh, J., Pastuglia, M., Bellini, C., Grandjean, O., and Bouchez, D. (2002). The Arabidopsis TONNEAU2 gene encodes a putative novel protein phosphatase 2A regulatory subunit essential for the control of the cortical cytoskeleton. Plant Cell **14**: 833–845.

Campos, R., Goff, J., Rodriguez-Furlan, C., and Van Norman, J.M. (2020). The Arabidopsis receptor kinase IRK Is polarized and represses specific cell divisions in roots. Dev. Cell **52**: 183–195.e4.

Caño-Delgado, A., Yin, Y., Yu, C., Vafeados, D., Mora-García, S., Cheng, J.-C., Nam, K.H., Li, J., and Chory, J. (2004). BRL1 and BRL3 are novel brassinosteroid receptors that function in vascular differentiation in Arabidopsis. Development **131**: 5341–5351.

Chaiwanon, J., Wang, W., Zhu, J.-Y., Oh, E., and Wang, Z.-Y. (2016). Information integration and communication in plant growth regulation. Cell **164**: 1257–1268.

Clough, S.J. and Bent, A.F. (1998). Floral dip: a simplified method for Agrobacterium-mediated transformation of Arabidopsis thaliana. Plant J. **16**: 735–743.

Correll, M.J. and Kiss, J.Z. (2005). The roles of phytochromes in elongation and gravitropism of roots. Plant Cell Physiol. **46**: 317–323.

Czechowski, T., Stitt, M., Altmann, T., Udvardi, M.K., and Scheible, W.-R. (2005). Genome wide identification and testing of superior reference genes for transcript normalization in Arabidopsis. Plant Physiol. **139**: 5–17.

Dietrich, D. et al. (2017). Root hydrotropism is controlled via a cortex-specific growth mechanism. Nat Plants **3**: 17057.

Diévart, A. and Clark, S.E. (2003). Using mutant alleles to determine the structure and function of leucine-rich repeat receptor-like kinases. Curr. Opin. Plant Biol. **6**: 507–516.

Dolan, L., Janmaat, K., Willemsen, V., Linstead, P., Poethig, S., Roberts, K., and Scheres, B. (1993). Cellular organisation of the Arabidopsis thaliana root. Development **119**: 71–84.

Dyson, R.J. et al. (2014). Mechanical modelling quantifies the functional importance of outer tissue layers during root elongation and bending. New Phytol. **202**: 1212–1222.

Facette, M.R., Rasmussen, C.G., and Van Norman, J.M. (2018). A plane choice: coordinating timing and orientation of cell division during plant development. Curr. Opin. Plant Biol. **47**: 47–55.

Friml, J., Wiśniewska, J., Benková, E., Mendgen, K., and Palme, K. (2002). Lateral relocation of auxin efflux regulator PIN3 mediates tropism in Arabidopsis. Nature **415**: 806– 809.

Grabov, A., Ashley, M.K., Rigas, S., Hatzopoulos, P., Dolan, L., and Vicente-Agullo, F. (2005). Morphometric analysis of root shape. New Phytol. **165**: 641–651.

Hajný, J. et al. (2020). Receptor kinase module targets PIN-dependent auxin transport during canalization. Science **370**: 550–557.

Hodge, A., Berta, G., Doussan, C., Merchan, F., and Crespi, M. (2009). Plant root growth, architecture and function. Plant Soil **321**: 153–187.

Kleine-Vehn, J., Ding, Z., Jones, A.R., Tasaka, M., Morita, M.T., and Friml, J. (2010). Gravity-induced PIN transcytosis for polarization of auxin fluxes in gravity-sensing root cells. Proc. Natl. Acad. Sci. U. S. A. **107**: 22344–22349.

Koncz, C., Németh, K., Rédei, G.P., and Schell, J. (1992). T-DNA insertional mutagenesis in Arabidopsis. Plant Mol. Biol. **20**: 963–976.

Lee, J.-Y., Colinas, J., Wang, J.Y., Mace, D., Ohler, U., and Benfey, P.N. (2006). Transcriptional and posttranscriptional regulation of transcription factor expression in Arabidopsis roots. Proc. Natl. Acad. Sci. U. S. A. **103**: 6055–6060.

Lee, M.M. and Schiefelbein, J. (1999). WEREWOLF, a MYB-related protein in Arabidopsis, is a position-dependent regulator of epidermal cell patterning. Cell **99**: 473–483.

Marhava, P., Hoermayer, L., Yoshida, S., Marhavý, P., Benková, E., and Friml, J. (2019). Re-activation of stem cell pathways for pattern restoration in plant wound healing. Cell **177**: 957–969.e13.

Martinez, P., Luo, A., Sylvester, A., and Rasmussen, C.G. (2017). Proper division plane orientation and mitotic progression together allow normal growth of maize. Proc. Natl. Acad. Sci. U. S. A. **114**: 2759–2764.

Meyerowitz, E.M. (1997). Genetic control of cell division patterns in developing plants. Cell **88**: 299–308.

Paquette, A.J. and Benfey, P.N. (2005). Maturation of the ground tissue of the root is regulated by gibberellin and SCARECROW and requires SHORT-ROOT. Plant Physiol. **138**: 636– 640.

Rasmussen, C.G. and Bellinger, M. (2018). An overview of plant division-plane orientation. New Phytol. **219**: 505–512.

Sabatini, S., Heidstra, R., Wildwater, M., and Scheres, B. (2003). SCARECROW is involved in positioning the stem cell niche in the Arabidopsis root meristem. Genes Dev. **17**: 354– 358.

Sablowski, R. (2016). Coordination of plant cell growth and division: collective control or mutual agreement? Curr. Opin. Plant Biol. **34**: 54–60.

Scheres, B. and Benfey, P.N. (1999). Asymmetric cell divisions in plants. Annu. Rev. Plant Physiol. Plant Mol. Biol. **50**: 505–537.

Schneider, C.A., Rasband, W.S., and Eliceiri, K.W. (2012). NIH Image to ImageJ: 25 years of image analysis. Nat. Methods **9**: 671–675.

Shao, W. and Dong, J. (2016). Polarity in plant asymmetric cell division: Division orientation and cell fate differentiation. Dev. Biol. **419**: 121–131.

Shiu, S.H. and Bleecker, A.B. (2003). Expansion of the receptor-like kinase/Pelle gene family and receptor-like proteins in Arabidopsis. Plant Physiol. **132**: 530–543.

Shiu, S.H. and Bleecker, A.B. (2001). Receptor-like kinases from Arabidopsis form a monophyletic gene family related to animal receptor kinases. Proc. Natl. Acad. Sci. U. S. A. **98**: 10763–10768.

Shpak, E.D., Berthiaume, C.T., Hill, E.J., and Torii, K.U. (2004). Synergistic interaction of three ERECTA-family receptor-like kinases controls Arabidopsis organ growth and flower development by promoting cell proliferation. Development **131**: 1491–1501.

Su, S.-H., Gibbs, N.M., Jancewicz, A.L., and Masson, P.H. (2017). Molecular mechanisms of root gravitropism. Curr. Biol. **27**: R964–R972.

Takano, J., Tanaka, M., Toyoda, A., Miwa, K., Kasai, K., Fuji, K., Onouchi, H., Naito, S., and Fujiwara, T. (2010). Polar localization and degradation of Arabidopsis boron transporters through distinct trafficking pathways. Proc. Natl. Acad. Sci. U. S. A. **107**: 5220–5225.

Vaahtera, L., Schulz, J., and Hamann, T. (2019). Cell wall integrity maintenance during plant development and interaction with the environment. Nat Plants **5**: 924–932.

Van Norman, J.M., Breakfield, N.W., and Benfey, P.N. (2011). Intercellular communication during plant development. Plant Cell **23**: 855–864.

Van Norman, J.M., Zhang, J., Cazzonelli, C.I., Pogson, B.J., Harrison, P.J., Bugg, T.D.H., Chan, K.X., Thompson, A.J., and Benfey, P.N. (2014). Periodic root branching in Arabidopsis requires synthesis of an uncharacterized carotenoid derivative. Proc. Natl. Acad. Sci. U. S. A. **111**: E1300–9.

Wang, J., Kucukoglu, M., Zhang, L., Chen, P., Decker, D., Nilsson, O., Jones, B., Sandberg, G., and Zheng, B. (2013). The Arabidopsis LRR-RLK, PXC1, is a regulator of secondary wall formation correlated with the TDIF-PXY/TDR-WOX4 signaling pathway. BMC Plant Biol. **13**: 94.

Willemsen, V., Bauch, M., Bennett, T., Campilho, A., Wolkenfelt, H., Xu, J., Haseloff, J., and Scheres, B. (2008). The NAC domain transcription factors FEZ and SOMBRERO control the orientation of cell division plane in Arabidopsis root stem cells. Dev. Cell **15**: 913–922.

Wu, S., O'Lexy, R., Xu, M., Sang, Y., Chen, X., Yu, Q., and Gallagher, K.L. (2016). Symplastic signaling instructs cell division, cell expansion, and cell polarity in the ground tissue of Arabidopsis thaliana roots. Proc. Natl. Acad. Sci. U. S. A. **113**: 11621–11626.

Wysocka-Diller, J.W., Helariutta, Y., Fukaki, H., Malamy, J.E., and Benfey, P.N. (2000). Molecular analysis of SCARECROW function reveals a radial patterning mechanism common to root and shoot. Development **127**: 595–603.

Yoshida, S., van der Schuren, A., van Dop, M., van Galen, L., Saiga, S., Adibi, M., Möller, B., Ten Hove, C.A., Marhavy, P., Smith, R., Friml, J., and Weijers, D. (2019). A SOSEKI based coordinate system interprets global polarity cues in Arabidopsis. Nat Plants **5**: 160– 166.

CHAPTER IV: Characterizing *crazy cortex*, an abnormal root ground tissue patterning phenotype in the *Arabidopsis* root

INTRODUCTION

In multicellular eukaryotes, regulating the timing and extent of cell divisions are key to the development and maintenance of tissue patterning and organ function. Observation of any disruption of the stereotypical organization of the Arabidopsis root meristem can be easily observed and is therefore an ideal model to study tissue patterning and development. In the Arabidopsis root, the pericycle which surrounds the vascular tissues within the stele, is surrounded from inside to outside by the endodermis, cortex, and epidermis (Dolan et al., 1993; Scheres et al., 1995). The cortex and endodermis are both cell types of the ground tissue and are derived from a single stem initial, the cortex/endodermal initial (CEI). The CEI divides to produce a daughter cell (CEID), which undergoes a periclinal cell division to produce endodermis towards the inside and the cortex towards the outside (Dolan et al., 1993; Benfey and Scheres, 2000). Additionally, later during development the endodermis divides periclinally to generate an additional layer of ground tissue, called middle cortex (Baum et al., 2002; Paquette and Benfey, 2005; Cui, 2016). Therefore, in the Arabidopsis root ground tissue, only endodermal and CEID cells typically undergo periclinal divisions with these cell divisions generating different root cell types.

We observed an unexpected mutant phenotype in plants expressing *pCO2:IRK:GFP* and segregating for *shr-2*, and upon characterization, we determined that this phenotype was caused by a dominant genetic lesion and was not associated with either the transgene insertion or with the *shr-2* loci. Thus, we named it *crazy cortex*

(*crz*) due to the presence of periclinal cell divisions in the cortex cell layer of the root meristem. The mechanisms regulating the timing and extent of periclinal cell divisions during ground tissue development have been extensively studied (Benfey and Scheres, 2000; Heidstra et al., 2004; Koizumi et al., 2012; Wu et al., 2016; Zhang et al., 2018), however only one gene involved in maintaining a single cell layer of cortex has been identified. This example is a mutation of the transcription factor *JACKDAW*, which results in cortex cells that divide periclinally to generate an additional cell layer and an increased number of endodermal and cortical cells in the radial axis (Welch et al., 2007). This suggests mutations with defects in periclinal divisions in the cortex are rare and could expand upon our understanding of oriented cell division regulation.

Here we report a novel phenotype in which the number of ground tissue cell layers in the root meristem is affected by a dominant mutation that results in periclinal divisions within the cortex cell layer. We examined the *crz* mutant phenotype and attempted to determine the location of the genetic lesion using bulk segregant analysis (BSA) and next-generation sequencing to identify the causative mutation. The additional GT layers in *crz* roots provide further evidence that IRK polarity is independent of cell identity and is instead directed by positional cues from adjacent cell layers. Our results suggest that repression of periclinal cortex cell division is genetically controlled and that *crz* plants can promote further understanding of how cellular position influences polarized protein localization.

RESULTS

crazy cortex roots have defects in ground tissue periclinal divisions

Upon examination of roots expressing *pCO2:IRK:GFP* and segregating for *shr-2*, we observed an abnormal phenotype in which there could be multiple periclinal divisions in the cortex (Figure 4.1A). In order to isolate this phenotype from the *shr-2* mutant background, plants exhibiting the *crz* phenotype were genotyped for *SHR* and plants with two wild type copies of *SHR* were propagated to the next generation. During this process we also selected plants that did not express the *pCO2:IRK:GFP* transgene to generate seeds that were putatively wild type except for the *crz* causative mutation(s). The *crz* root phenotype was present in plants that lacked the *pCO2:IRK:GFP* transgene and plants that were wild type for *SHR*, indicating that this phenotype was seperate from loci associated with either the insertion of the *pCO2:IRK:GFP* transgene or the *shr-2* mutation.

Detailed examination of *crz* roots revealed that several abnormal ground tissue cell division phenotypes occur. In putative homozygous lines, we observed 100% of the seedlings had abnormal ground tissue periclinal cell divisions with three distinct classes of abnormal phenotypes observed. First, 25% of the roots had two layers of ground tissue and one or more periclinal divisions that apparently originated in the cortex (Figure 4.1A). Second, we observed ~55% of roots with a single layer of ground tissue in which some cells had undergone a single periclinal division (Figure 4.1B); finally, ~20% the roots with a single layer of ground tissue with no cells that had undergone periclinal divisions (Figure 4.1C). This suggests either that the lesion causing the *crz* phenotype is

dominant and pleiotropic or that another locus is segregating in and is acting as a modifier within the genetic background.

Among lines that were putatively heterozygous at *crz* we observed similar abnormal GT phenotypes, with 25% of roots having a multilayered ground tissue, 25% single layer with a few periclinal divisions, 30% single layer no periclinal divisions, and 20% of roots having an apparently wild-type phenotype with two ground tissue layers with no periclinal cortical cell divisions. This phenotypic ratio is consistent with the *crz* mutation being dominant and perhaps having a dose effect. To test this hypothesis, individual roots from a putative homozygous population exhibiting each *crz* abnormal root phenotype were backcrossed to Col-0 (wild type). The progeny of Col-0 crossed with a *crz* plant with a single ground tissue layer, all showed the multiple periclinal cortical cell division phenotype. This suggests *crz* plants with the single ground tissue layer represent individuals with two copies of the genetic lesion that causes the *crz* phenotype. While progeny from Col-0 crossed with a *crz* multi-layered ground tissue plant were 50% wild type, and 50% multilayered ground tissue. These results indicate that the *crz* mutation is a dominant mutation and suggests that the presence of a single mutant copy leads to the multi-layered ground tissue phenotype, while a single layer of ground tissue phenotype was only observed when two mutant copies are present (Figure 4.1).

As the *crz* phenotype was discovered as a spontaneous genetic lesion, we sought to identify the causative mutation. Following my observation that when plants with the *crz* single ground tissue layer phenotype were backcrossed, the resulting

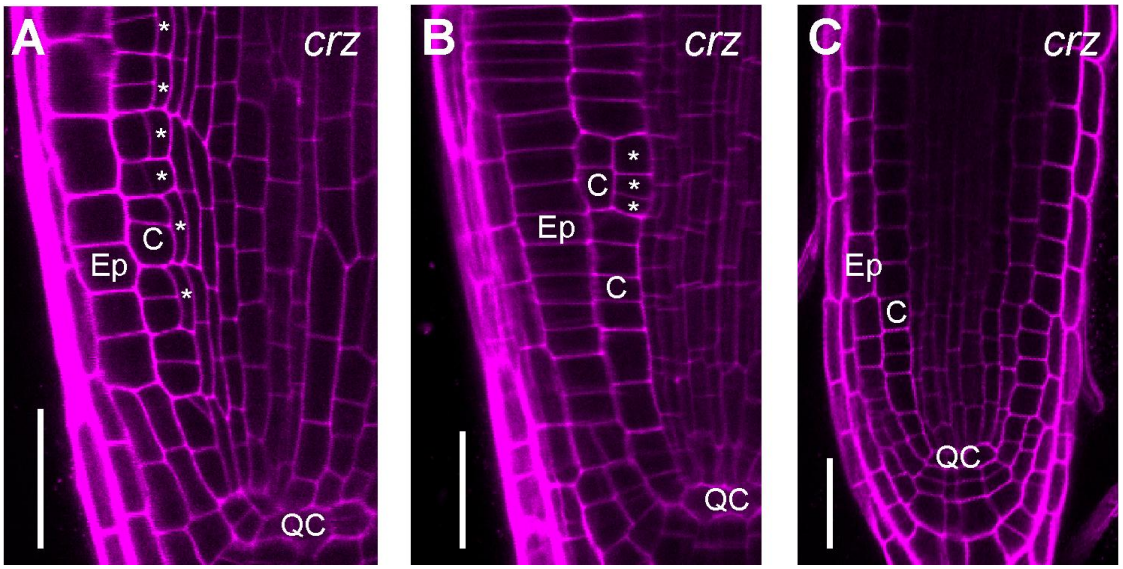

Figure 4.1 - *crz* roots have defects in ground tissue cell layer number.
Confocal micrographs of *crz* roots stained with propidium iodide (PI) exhibiting varying phenotypes. *crz* roots have ground tissue with (A) multiple layers, (B) single layer with a periclinal division, and (C) single layer with no periclinal divisions. Scale Bars: (A, B) 25μm, (C) 30μm. Abbreviations: Ep - Epidermis, C - putative cortex, QC - quiescent center, asterisks show periclinal divisions originating from the putative cortex.

progeny all had the *crz* multi-layered GT phenotype, I predicted that *crz* plants with a single ground tissue layer were homozygous for *crz*. A standard genetic cross was done with a putative *crz* homozygous plant, which is in the Columbia (Col-0) background, and a Landsberg *erecta* (L.*er*) plant to generate a mapping population. Using single sequence length polymorphisms (SSLP) markers between the Col-0 and L.*er* ecotypes I mapped the genetic region associated with the *crz* phenotype. These results indicated the causative region for *crz* phenotype was located on the bottom arm of Chromosome 5, close to the centromere. However, despite eliminating a large portion of the genome, we were not able to obtain sufficient data to further reduce the locus to a small enough size to begin testing candidate genes as causative in the *crz* phenotype.

To identify the causative gene, Next-Gen sequencing of ~150 putative *crz* mutant individuals (plants with the single layer of GT phenotype) mapped the mutation to a ~200kb region on the bottom of Chromosome 5 near the centromere. This is consistent with our SSLP mapping data, however the sequencing data also suggested a region on Chromosome 4 was segregating as a potential genetic modifier in these *crz* individuals. This data also suggested that individuals selected for genotyping based on the phenotype with a single layer of ground tissue (Figure 4.1C) were not homozygous for a mutation at the putative *crz* locus on 5B. Thus, additional phenotypic analyses need to be conducted to reliably select *crz* mutants based on an abnormal GT phenotype alone.

CYCD6;1 is expressed during the periclinal divisions in *crz* ground tissue

To understand if the periclinal divisions originating from the presumptive cortex occur through a previously characterized cell cycle protein specific to ground tissue formative divisions, we investigated the expression of *pCYCD6;1:erGFP* in *crz* roots. Periclinal cell divisions in the ground tissue occur as part of normal development, however in *Arabidopsis*, these divisions typically occur only when the CEID divides to generate endodermis and cortex, and when the endodermis divides to generate middle cortex. Prior to these periclinal divisions, the *pCYCD6;1:erGFP* reporter is active and can be used as a marker of periclinal ground tissue cell divisions (Sozzani et al., 2010, Bertolotti et al., 2021). Expression of *pCYCD6;1:erGFP* is specific to formative cell divisions in the ground tissue, and is typically not expressed in the cortex (Sozzani et al., 2010). Because *pCYCD6;1* activity is ground tissue specific, we proposed that it might be associated with aberrant cortical cell divisions in *crz* roots.

To determine whether the periclinal divisions in *crz* roots are similar to other ground tissue periclinal divisions and expressed *CYCD6;1*, we crossed *crz* plants with *pCYCD6;1:GFP*. Upon examination of plants that were homozygous for the *pCYCD6;1* reporter and homozygous for *crz*, I found that *pCYCD6;1:GFP* was highly active in the cortex in *crz* roots prior to and following periclinal divisions at 7 dps (Figure 4.2). This suggests that these cells in *crz* have ground tissue identity, that SHR is present and active in these cells as CYCD6;1 activity is downstream of SHR (Sozzani et al., 2010), and/or that the pathway(s) regulating endodermal periclinal divisions and cortical periclinal divisions in *crz* roots similarly converge on *pCYCD6;1* activity prior to

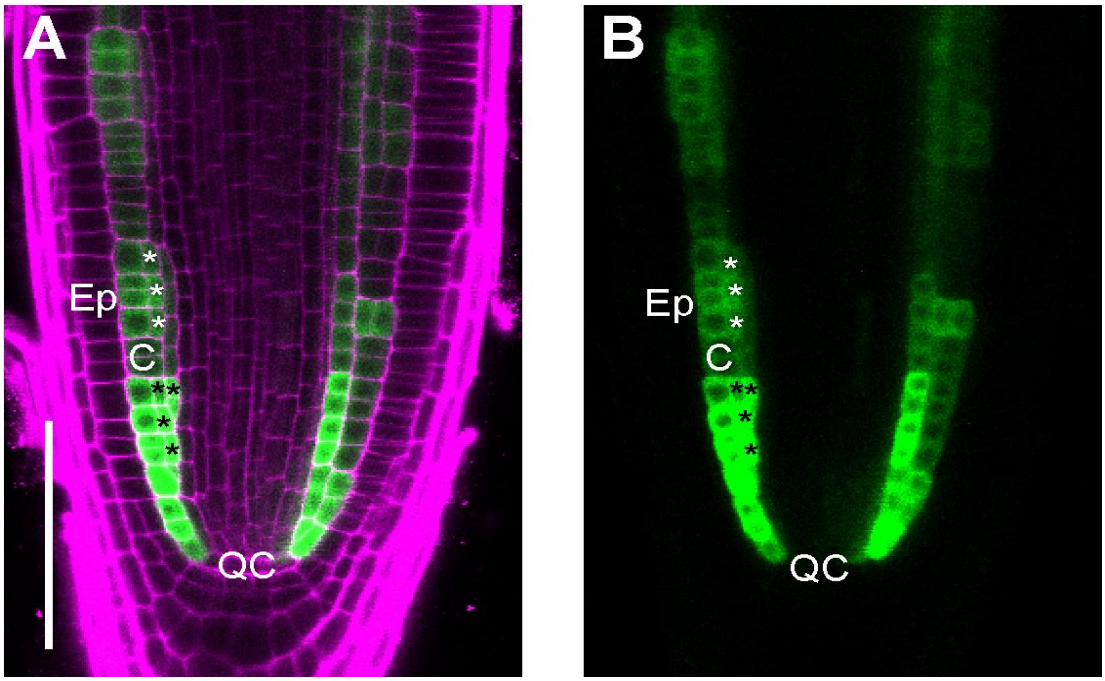

Figure 4.2 - *pCYCD6;1* is expressed in the cortex during periclinal divisions in *crz*. *crz* roots expressing *pCYCD6;1:GFP* at 7dps with (A) Merged (PI and GFP) and (B) GFP channel alone. showing misexpresion of *CYCD6;1* in the putative cortex/ground tissue. Abbreviations: Ep - Epidermis, C - putative cortex, QC - quiescent center, asterisks show periclinal divisions originating from the putative cortex. Scale Bar: 75µm

occurrence of these cell divisions. Furthermore, we observed expression of *pCYCD6;1:GFP* in the cell layer to the inside of the putative cortex layer (putative endodermal cells), however, these cells do not have periclinal divisions, suggesting that activity of *pCYCD6;1* alone was not sufficient to generate a periclinal division in the *crz* ground tissue. *pCYCD6;1* activity in these cells indicates the periclinal divisions of the putative cortex in *crz* roots has similarity to formative divisions of the CEI/CEID and endodermis.

crz can serve as a tool to further understand IRK polar localization

As mentioned previously, phenotypic analysis of *crz* roots led to the observation that individual plants from a single parent have one of three abnormal ground tissue phenotypes: two GT cell layers with putative cortex cells showing multiple periclinal divisions, or a single layer of ground tissue with or without periclinal divisions. Occasionally, individual *crz* roots displayed all these abnormal phenotypes, which can be used to study IRK localization in the context of variable GT layer number within a single root. In wild-type, IRK-GFP localizes to the inner polar

domain in the cortex (Campos et al., 2020), while in *shr* and *scr* mutants, when a single layer of ground tissue with cortex identity is present, IRK-GFP localizes to the rootward/shootward polar domains (Campos et al., 2020). *scr* mutants have the potential for a periclinal cell division to generate an additional ground tissue layer (Paquette and Benfey, 2005) and upon the formation of two ground tissue layers in *scr*, IRK-GFP shows lateral polarity with localization to the inner polar domain in the outermost cell and

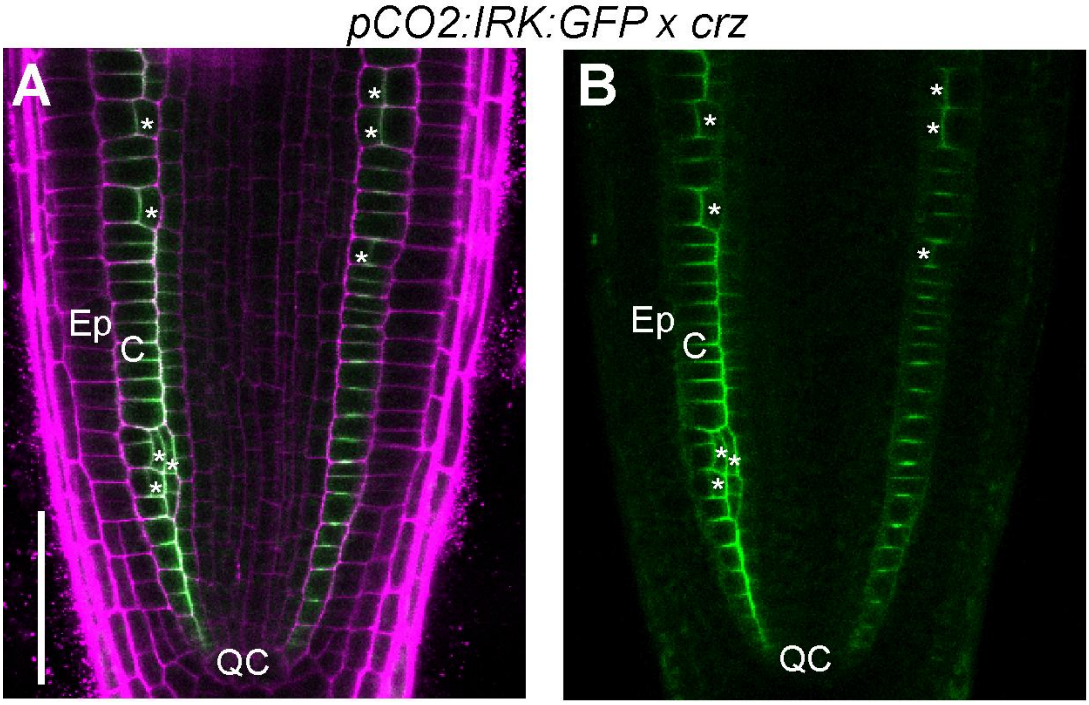

Figure 4.3 - IRK-GFP polar localization in *crz* demonstrates how positional information determines IRK polarity. Expression of *pCO2:IRK:GFP* in *crz* roots with (A) Merged (PI + GFP) and (B) GFP alone, showing IRK-GFP polar localization is different depending on the number of ground tissue layers present in *crz*. Abbreviations: Ep - Epidermis, C - putative cortex, QC - quiescent center, asterisk - periclinal division originating from the putative cortex. Scale Bar: 50μm

to the outer polar domain in the innermost ground tissue cell (Campos et al., 2020). These results indicated that IRK polarity was informed by information from neighboring cell types. Only when two layers of ground tissue are present does IRK-GFP localize to the inner polar domain in the outermost ground tissue cell type, to the outer polar domain in the innermost cell of the ground tissue, and rootward/shootward when a single layer of ground tissue is present (Campos et al., 2020).

Based on these observations in *scr*, *shr* and in the middle cortex of WT roots, I predicted that if positional information informed IRK localization, then IRK-GFP localization in *crz* mutants would change based on the number of ground tissue cell layers present. Upon examination of *crz* roots expressing *pCO2:IRK:GFP*, IRK-GFP was localized to the rootward/shootward polar domains when a single layer of ground tissue is present, while lateral polarity was observed in cells immediately adjacent to either the epidermis or pericycle when two or more layers of ground tissue are present (Figure 4.3). Additionally, we observed that IRK-GFP is non-polar in cells positioned between two or more adjacent (presumptive GT) cell layers in *crz* roots. These observations are consistent with our previous findings that when a single layer of ground tissue is present IRK-GFP localizes to the rootward/shootward polar domains, however lateral polarity occurs when there are two layers in the ground tissue. Finally, we found that IRK-GFP was nonpolar when expressed in middle cortex (Campos et al., 2020) and in GT cell layers of any number as long as other GT cells were peripheral to them. This suggests when a GT cell is between two or more ground tissue cell layers then IRK-GFP localization will be nonpolar. These findings further support our hypothesis that IRK polar localization is determined by information from locally adjacent cell types.

DISCUSSION

With the discovery of the *crz* phenotype, we have the opportunity to further understand how periclinal divisions are controlled during root ground tissue development, particularly in cells that do not typically divide in this orientation. Our preliminary phenotypic analysis showed that *crz* roots have defects in ground tissue patterning, exhibiting abnormal periclinal divisions in the cortex and/or the presence of a single layer of ground tissue. It is unclear whether this single layer of ground tissue has cortex identity, similar to *shr* mutants, or mixed cortical/endodermal identity similar to *scr* mutants (Di Laurenzio et al., 1996). Furthermore, the *crz* mutation appears to only affect the root ground tissue as the *crz* plants otherwise grow normally without detectable morphological defects.

We determined through backcrossing that the *crz* phenotype was likely caused by a dominant mutation, and therefore it was likely that the observed phenotype is caused by a gain-of-function mutation. Although the causative mutation for the *crz* phenotype is not yet known, Next-Gen sequencing results a region encompassing ~40 candidate genes was identified on Chromosome 5 associated with the phenotype. A review of their predicted functions did not lead to a clear candidate gene(s) that one would predict to be causative for the *crz* phenotype. *crz* individuals were selected for mapping based on the presence of a single layer of ground tissue, however these plants were not homozygous mutant at the locus on 5B and showed a genetic modifier found on Chromosome 4. This indicates that additional phenotypic analysis will be required

prior to another attempt to locate the causative mutation using whole genome sequencing so that *crz* homozygous plants are selected for sequencing.

Finally, the identity of the ground tissue cells in *crz* plants remains an open question. Typically, cortex cells do not divide periclinally and although periclinal divisions in the root are typically formative and result in a daughter cells of different fates (Dolan et al., 1993; van den Berg et al., 1998; Cederholm et al., 2012), we know these daughter cells are likely GT cells based on activity of *pCYCD6;1* and *pCO2* activity which is specific to cortical cells in the root meristem. In Arabidopsis, the endodermis can undergo a periclinal division to generate middle cortex, however, in other plant species, such as *Solanum lycopersicum* and *Oryza sativa* the endodermis undergoes multiple rounds of periclinal divisions to generate multiple layers of middle cortex (Eshed et al., 2001; Coudert et al., 2010). Although the cells in *crz* appear to be derived from a cortical periclinal divisions, we predict daughter cells to the inside of the cortex have middle cortex identity regardless of the number of cell layers, and that the endodermis, if present, would retain its identity and be present as a single layer. To begin addressing the question of cell identity, cell type-specific reporters will be crossed with *crz* to determine the identity of the cells which result from the periclinal GT divisions in *crz*. Determination of the identity of these cells is especially important as periclinal divisions in the cortex do not occur in wild type, therefore if daughter cells from cortical periclinal divisions and endodermal periclinal divisions both result in MC formation then this would further support the hypothesis that positional information, not linage determines cell identity of formative divisions in the GT.

EXPERIMENTAL PROCEDURES

Plant materials and growth conditions

Seeds were surface sterilized with chlorine gas, then plated on media (pH 5.7) containing 1% (BD Difco™) Agar and 0.5g/L MES (EMD), supplemented with 1% sucrose w/v and 1x Murashige and Skoog (MS, Caisson labs) basal salts. Plates were sealed with parafilm and stratified on plates in the dark at 4°C for 48-72 hours and then placed vertically in a Percival growth chamber, with 16h light/8h dark cycle at a constant temperature of 22°C.

Confocal microscopy and analysis of fluorescent reporters

Roots were stained with ~10 μM propidium iodide (PI) solubilized in water for 1-2 min and visualized via laser scanning confocal microscopy on a Leica SP8 upright microscope housed in the Van Norman lab. Fluorescence signals were visualized as follows: GFP (excitation 488 nm, emission 492-530 nm), and PI (excitation 536 nm, emission 585-660 nm). All confocal images are median longitudinal optical sections, acquired in the root meristematic zone.

Phenotypic characterization of *crz* plants

The *crz* phenotype was isolated from *shr-2* and *pCO2:IRK:GFP* in a population that was segregating for all genotypes. Roots were screened via fluorescence microscopy for the presence of IRK-GFP and then individuals without fluorescence were then genotyped to be wild type at *SHR* via PCR. These plants were then

phenotyped via confocal microscopy at 4-7dps on standard media plates sealed with parafilm, with no differences in phenotype observed due to plant age. *crz* plants were scored based on defects observed in ground tissue patterning, *crz* mutant lines were determined by the absence of any ground tissue with a wild-type phenotype.

Figure construction

For use in figures, raw confocal images were converted to .TIF format using Leica software (LASX) and were assembled in Adobe Photoshop. Figures containing images and schematics were assembled in Adobe Illustrator.

Genetic Mapping of *crz* by PCR

crz plants that were previously backcrossed to Col-0 were crossed with *Landsberg erecta* (Ler) plants and F1 progeny were genotyped via confocal microscopy for presence of ground tissue defects, and then transplanted on soil to self propagate. The segregating F2 population was screened for putative *crz* mutants at 7dps with a single layer of ground tissue. DNA from ~30 putative *crz* mutants was extracted and then used as a template along with Col-0, Ler, and Col-0/Ler heterozygous plants for genetic mapping by use of SSLP (single sequence length polymorphism) primers. For each SSLP primer a PCR product of different length was generated based on the ecotype of the plant in that genomic region. As the *crz* phenotype is observed in the Col-0 background, we predicted that the phenotype would segregate with the ecotype.

Next-Gen sequencing of *crz*

Approximately 150 *crz* plants with a single layer of ground tissue were selected via confocal microscopy, snap frozen in liquid nitrogen at 5-7dps and then ground with pestle and mortar. DNA was extracted using the C-TAB protocol (Springer, 2010) and pooled for use with NEBNext DNA Library Prep Master Mix Set for Illumina (E6040). DNA extraction and library prep was performed with assistance and guidance from Angelica Guergo and Dr. Jacob Landis. Resulting data was analyzed by Angelica Guercio and Dr. Dan Koenig and presented to the Van Norman lab.

REFERENCES

Baum, S.F., Dubrovsky, J.G., and Rost, T.L. (2002). Apical organization and maturation of the cortex and vascular cylinder in Arabidopsis thaliana (Brassicaceae) roots. Am. J. Bot. **89**: 908–920.

Benfey, P.N. and Scheres, B. (2000). Root development. Curr. Biol. **10**: R813–5.

van den Berg, C., Weisbeek, P., and Scheres, B. (1998). Cell fate and cell differentiation status in the Arabidopsis root. Planta **205**: 483–491.

Bertolotti, G., Unterholzner, S.J., Scintu, D., Salvi, E., Svolacchia, N., Di Mambro, R., Ruta, V., Linhares Scaglia, F., Vittorioso, P., Sabatini, S., Costantino, P., and Dello Ioio, R. (2021). A PHABULOSA-controlled genetic pathway regulates ground tissue patterning in the Arabidopsis root. Curr. Biol. **31**: 420–426.e6.

Campos, R., Goff, J., Rodriguez-Furlan, C., and Van Norman, J.M. (2020). The Arabidopsis receptor kinase IRK Is polarized and represses specific cell divisions in roots. Dev. Cell **52**: 183–195.e4.

Cederholm, H.M., Iyer-Pascuzzi, A.S., and Benfey, P.N. (2012). Patterning the primary root in Arabidopsis. Wiley Interdiscip. Rev. Dev. Biol. **1**: 675–691.

Coudert, Y., Périn, C., Courtois, B., Khong, N.G., and Gantet, P. (2010). Genetic control of root development in rice, the model cereal. Trends Plant Sci. **15**: 219–226.

Cui, H. (2016). Middle cortex formation in the root: an emerging picture of integrated regulatory mechanisms. Mol. Plant **9**: 771–773.

Di Laurenzio, L., Wysocka-Diller, J., Malamy, J.E., Pysh, L., Helariutta, Y., Freshour, G., Hahn, M.G., Feldmann, K.A., and Benfey, P.N. (1996). The SCARECROW gene regulates an asymmetric cell division that is essential for generating the radial organization of the Arabidopsis root. Cell **86**: 423–433.

Dolan, L., Janmaat, K., Willemsen, V., Linstead, P., Poethig, S., Roberts, K., and Scheres, B. (1993). Cellular organisation of the Arabidopsis thaliana root. Development **119**: 71–84.

Eshed, Y., Baum, S.F., Perea, J.V., and Bowman, J.L. (2001). Establishment of polarity in lateral organs of plants. Curr. Biol. **11**: 1251–1260.

Heidstra, R., Welch, D., and Scheres, B. (2004). Mosaic analyses using marked activation and deletion clones dissect Arabidopsis SCARECROW action in asymmetric cell division. Genes Dev. **18**: 1964–1969.

Koizumi, K., Hayashi, T., Wu, S., and Gallagher, K.L. (2012). The SHORT-ROOT protein acts as a mobile, dose-dependent signal in patterning the ground tissue. Proc. Natl. Acad. Sci. U. S. A. **109**: 13010–13015.

Nakajima, K., Sena, G., Nawy, T., and Benfey, P.N. (2001). Intercellular movement of the putative transcription factor SHR in root patterning. Nature 413: 307–311.

Paquette, A.J. and Benfey, P.N. (2005). Maturation of the ground tissue of the root is regulated by gibberellin and SCARECROW and requires SHORT-ROOT. Plant Physiol. **138**: 636–640.

Scheres, B., Di Laurenzio, L., Willemsen, V., Hauser, M.T., Janmaat, K., Weisbeek, P., and Benfey, P.N. (1995). Mutations affecting the radial organisation of the Arabidopsis root display specific defects throughout the embryonic axis. Development **121**: 53–62.

Sozzani, R., Cui, H., Moreno-Risueno, M.A., Busch, W., Van Norman, J.M., Vernoux, T., Brady, S.M., Dewitte, W., Murray, J.A.H., and Benfey, P.N. (2010). Spatiotemporal regulation of cell-cycle genes by SHORTROOT links patterning and growth. Nature **466**: 128–132.

Springer, N.M. (2010). Isolation of plant DNA for PCR and genotyping using organic extraction and CTAB. Cold Spring Harb. Protoc. **2010**: db.prot5515.

Welch, D., Hassan, H., Blilou, I., Immink, R., Heidstra, R., and Scheres, B. (2007). Arabidopsis JACKDAW and MAGPIE zinc finger proteins delimit asymmetric cell division and stabilize tissue boundaries by restricting SHORT-ROOT action. Genes Dev. **21**: 2196–2204.

Wu, S., O'Lexy, R., Xu, M., Sang, Y., Chen, X., Yu, Q., and Gallagher, K.L. (2016). Symplastic signaling instructs cell division, cell expansion, and cell polarity in the ground tissue of Arabidopsis thaliana roots. Proc. Natl. Acad. Sci. U. S. A. **113**: 11621–11626.

Zhang, X., Zhou, W., Chen, Q., Fang, M., Zheng, S., Scheres, B., and Li, C. (2018). Mediator subunit MED31 is required for radial patterning of Arabidopsis roots. Proc. Natl. Acad. Sci. U. S. A.

CHAPTER V: Discussion and future directions

Controlling the timing and progression of developmental events across cell types and tissues requires both perception and transduction of cues by individual cells. Polarized (directional) signaling between neighboring cell types has been implied to control the timing and progression of various developmental events in plants (Van Norman et al., 2011). Characterization of IRK and PXC2 provides further links between cell division, cell polarity, and cell-cell communication during root tissue development. Our results indicate that oriented cell division and lateral cell polarity are connected by IRK and PXC2 function in root GT patterning. Furthermore, regulation of periclinal cell divisions in the root's cortex cell layer is disrupted in *crz* plants, suggesting that the ability of these cells to undergo periclinal division is under genetic control. Identification of the gene(s) associated to the *crz* phenotype will allow us to begin to understand and further dissect the mechanisms controlling oriented cell divisions in plants.

Identifying the causative gene(s) for the abnormal *crz* phenotype

Characterization of the *crz* mutant phenotype revealed a novel phenotype in which a dominant, putative gain-of-function genetic lesion resulted in periclinal divisions in the presumptive cortex cell layer. In putative homozygous lines, we identified 3 distinct classes of abnormal phenotypes: one with excess periclinal divisions in the GT and two with fewer. I identified those with the single layer of GT as the homozygotes, however, based on the DNA sequencing data, this conclusion was erroneous. This indicates that the phenotypic ratios need to be carefully re-examined and segregation of a genetic

modifier in the background included into the hypothesis testing. Although the sequencing data based on the single layer GT phenotype did map the *crz* genetic lesion to a region with ~40 candidate genes on 5B, it also identified another region on Chromosome 4. Based on these data, identification of the *crz* lesion(s) was not going to be straightforward with the selected individuals and would require extensive reexamination of the phenotypes, out/map crosses, and another round of sequencing.

Polar localization of IRK and PXC2 to specific PM domains

IRK and PXC2 localize to similar PM domains when expressed in specific cell types and we have established that information from immediately adjacent cells (in the radial axis) and not cell identity per se informs IRK and PXC2 polar localization. Yet, it is unclear how relative positional information is perceived by a given cell or how that information is transduced to ultimately inform IRK/PXC2 polar localization. Additionally, it is not clear whether this communication between adjacent cell layers occurs via apoplastic or symplastic signaling pathways or if perception of an extrinsic signal by IRK/PXC2 themselves is required for their localization. To test if symplastic signaling informs IRK and/or PXC2 polarity, plants expressing *pIRK:IRK:GFP* and/or *pPXC2:PXC2:GFP* can be crossed with plants expressing an inducible callose synthase gene in the endodermis (*pSCR:icals3-m)* (Vatén et al., 2011). Induction of its expression would block symplastic communication between the endodermis, CEI/CEID, and QC and neighboring cell layers. If upon callose induction, we observed a change in IRK/PXC2 localization it would suggest that symplastic signaling through plasmodesmata is required for polar accumulation at specific PM domains. However, if we observed no

change in IRK/PXC2 polar localization, it would suggest that signaling through plasmodesmata is not required for their polar localization. Determination of the mode of delivery of the extrinsic signal could assist in identifying additional components of the machinery necessary for polar localization of IRK/PXC2 and other polarized proteins.

In addition to investigating the cellular requirements for IRK/PXC2 polar localization, we would also like to determine whether intramolecular features of the IRK/PXC2 proteins are required for their polarity. IRK and PXC2 are classified as atypical kinases meaning their kinase domains contain non-conserved amino acid residues at key positions (Nolen et al., 2004; Castells and Casacuberta, 2007), and while IRK has been shown to have autophosphorylation activity in E. *coli* (Hattan et al., 2004), PXC2 lacks autophosphorylation activity (Hajný et al., 2020). We have determined that the IRK intracellular kinase and juxtamembrane domains are not necessary for its polar localization (Rodriguez-Furlan et al., under revision for Nature Communications). Although this has yet to be tested for PXC2, we expect that the results will be similar. As the intracellular domains of IRK are not required for its polar localization, it is unlikely that localization is based on a cytoplasmic protein partner and may instead be due to targeted secretion of IRK to the membrane or interaction with another protein through its transmembrane or extracellular domains. These truncated versions of IRK and PXC2 can also be functionally assessed to determine which protein domains are most important for their functions in root development.

Expression of *IRK* during MC development

In Chapter II, I conduct a preliminary assessment of the activity of the *IRK* promoter during MC formation. Because SHR accumulation decreases in endodermal cells prior to the periclinal division to form MC (Koizumi et al., 2012) and *IRK* is a putative downstream target of SHR (Sozzani et al., 2010), we predict that *IRK* promoter activity would decrease as endodermal cells prepare to divide. This is consistent with the observation that in *irk* mutants there are excess endodermal periclinal divisions. I find that *pIRK:erGFP* expression appears to be unchanged prior to endodermal periclinal divisions that lead to MC formation. These preliminary results suggest that a reduction in *IRK* promoter activity does not preceed these divisions. However, given the preliminary nature of these results, it would be premature to make a solid conclusion without further experiments. If similar results are obtained from future replicates of this experiment, it may suggest either that a decrease in SHR accumulation is not a negative transcriptional regulator of *IRK*, that the persistent nature of erGFP precludes an observable reduction in *pIRK* activity during short time scales, and/or that promoter activity is not the primary means of controlling IRK accumulation and function. Given that IRK is a transmembrane receptor, regulation of its activity may occur at the protein level, perhaps in terms of abundance at the PM. Activity of *pIRK* and IRK accumulation at the PM is restricted to the root meristem (Campos et al., 2020), which coincides with its function to restrict endodermal LADs, as it is currently unknown how *IRK* expression is restricted to the meristem investigation of how *pIRK* is transcriptionally repressed in cells outside of the meristem may help to further understand IRK function.

Probing function of IRK, PXC2 and other closely related LRR-RLKs

pxc2 mutant roots have increased stele area compared to wild type indicating that PXC2 functions to restrict stele area. As the *pxc2* mutant phenotype was only observed when seedlings are grown on media with lower concentrations of nutrients, we concluded that IRK has a more dominant role to limit stele area as *irk-4* mutants have a larger stele when grown on standard media. In *irk-4 pxc2-3* double mutants, an enhanced increase in endodermal LADs and stele area is observed indicating that IRK and PXC2 act redundantly to limit these processes. Despite their partially redundant functions, we show that contrary to IRK misexpression of PXC2-GFP in the endodermis is not sufficient to fully compensate for loss of IRK function. The inability of PXC2-GFP to rescue *irk-4* phenotypes leads to a question of why these proteins are not functionally equivalent. Is this due to spatiotemporal differences in expression levels or protein accumulation? Or perhaps it is due to differences in biochemical activity of the proteins themselves? Further exploration of PXC2 functional equivalency for IRK would involve expressing PXC2 driven by *pIRK* or a ubiquitously expressing promoter in *irk-4* mutants. Additionally, determining if expression of *IRK* driven by *pPXC2* and/or a xylem specific promoter such as *TARGET OF MONOPTEROS5* (*TMO5*) (De Rybel et al., 2013) could fully rescue the *pxc2-3* mutant stele area phenotype, as endogenously in the vasculature *PXC2* is only expressed in the root xylem.

Because functional redundancies exist between closely related IRK and PXC2, an important question to address is whether characterization of higher order mutants with other closely related genes in the subfamily (Shiu and Bleecker, 2001) would reveal

additional functions for these receptors. We predict that disruption of additional genes related to *IRK* and *PXC2* would result in further enhancement of the *irk-4 pxc2-3* phenotypes with higher order mutant plants potentially exhibiting further disruption of root ground tissue patterning and gravitropic response and/or abnormal phenotypes beyond the root.

REFERENCES

Campos, R., Goff, J., Rodriguez-Furlan, C., and Van Norman, J.M. (2020). The Arabidopsis receptor kinase IRK Is polarized and represses specific cell divisions in roots. Dev. Cell **52**: 183–195.e4.

Castells, E. and Casacuberta, J.M. (2007). Signalling through kinase-defective domains: the prevalence of atypical receptor-like kinases in plants. J. Exp. Bot. **58**: 3503–3511.

Hajný, J. et al. (2020). Receptor kinase module targets PIN-dependent auxin transport during canalization. Science **370**: 550–557.

Hattan, J., Kanamoto, H., Takemura, M., Yokota, A., and Kohchi, T. (2004). Molecular characterization of the cytoplasmic interacting protein of the receptor kinase IRK expressed in the inflorescence and root apices of Arabidopsis. Biosci. Biotechnol. Biochem. **68**: 2598–2606.

Koizumi, K., Hayashi, T., Wu, S., and Gallagher, K.L. (2012). The SHORT-ROOT protein acts as a mobile, dose-dependent signal in patterning the ground tissue. Proc. Natl. Acad. Sci. U. S. A. **109**: 13010–13015.

Nolen, B., Taylor, S., and Ghosh, G. (2004). Regulation of protein kinases: controlling activity through activation segment conformation. Mol. Cell **15**: 661–675.

Shiu, S.H. and Bleecker, A.B. (2001). Receptor-like kinases from Arabidopsis form a monophyletic gene family related to animal receptor kinases. Proc. Natl. Acad. Sci. U. S. A. **98**: 10763–10768.

Sozzani, R., Cui, H., Moreno-Risueno, M.A., Busch, W., Van Norman, J.M., Vernoux, T., Brady, S.M., Dewitte, W., Murray, J.A.H., and Benfey, P.N. (2010). Spatiotemporal regulation of cell-cycle genes by SHORTROOT links patterning and growth. Nature **466**: 128–132.

Van Norman, J.M., Breakfield, N.W., and Benfey, P.N. (2011). Intercellular communication during plant development. Plant Cell **23**: 855–864.

Vatén, A. et al. (2011). Callose biosynthesis regulates symplastic trafficking during root development. Dev. Cell **21**: 1144–1155.